Nature Communications

https://doi.org/10.1038/s41467-026-72734-9

Article in Press

Early-life *Wnt4* expressing colon stromal cells orchestrate lifelong mucosal homeostasis via BMP-driven iNKT cell imprinting

Received: 25 June 2025

Accepted: 23 April 2026

Cite this article as: Lin, X., Lee, C.H.-J., Zhang, T. *et al.* Early-life *Wnt4* expressing colon stromal cells orchestrate lifelong mucosal homeostasis via BMP-driven iNKT cell imprinting. *Nat Commun* (2026). https://doi.org/10.1038/s41467-026-72734-9

Xi Lin, Chloe Hyun-Jung Lee, Ting Zhang, Agne Antanaviciute, Thomas Hanley, Jonathan N. Glickman, Nikhila S. Bharadwaj, Vicki Rosen, Jenny E. Gumperz, Matthew K. Waldor, Alison Simmons, Thomas Gensollen & Richard S. Blumberg

Early-life *Wnt4* expressing colon stromal cells orchestrate lifelong mucosal homeostasis via BMP-driven iNKT cell imprinting

Xi Lin[1], Chloe Hyun-Jung Lee[2,3], Ting Zhang[4], Agne Antanaviciute[2,3], Thomas Hanley[1], Jonathan N. Glickman[5], Nikhila S. Bharadwaj[6], Vicki Rosen[7], Jenny E. Gumperz[6], Matthew K. Waldor[8,9,10], Alison Simmons[2], Thomas Gensollen[11, †], Richard S. Blumberg[1, †, *]

Affiliations:

1. Division of Gastroenterology, Department of Medicine, Brigham and Women's Hospital, Harvard Medical School, 75 Francis Street, Boston, MA, USA.
2. Medical Research Council Translational Immune Discovery Unit, MRC Weatherall Institute of Molecular Medicine, Radcliffe Department of Medicine, John Radcliffe Hospital, University of Oxford, Oxford OX3 9DS, UK
3. MRC Center for Computational Biology, Weatherall Institute of Molecular Medicine, University of Oxford, Oxford, UK
4. Department of Molecular Microbiology, Washington University School of Medicine, St. Louis, MO, USA.
5. Department of Pathology, Massachusetts General Hospital, Harvard Medical School, Boston, MA, USA.
6. Department of Medical Microbiology and Immunology, University of Wisconsin School of Medicine and Public Health, Madison, Wisconsin, USA.
7. Department of Developmental Biology, Harvard School of Dental Medicine, Boston, MA, USA
8. Division of Infectious Diseases, Brigham and Women's Hospital, Boston, MA, USA.
9. Department of Microbiology, Harvard Medical School, Boston, MA, USA.
10. Howard Hughes Medical Institute, Boston, MA, USA.
11. Institut de Pharmacologie et de Biologie Structurale (IPBS), Université de Toulouse, CNRS, Université Toulouse III - Paul Sabatier (UT3), Toulouse, France.

† These authors jointly supervised this work

* Corresponding author, rblumberg@bwh.harvard.edu

Abstract

The early-life intestinal microenvironment plays a pivotal role in shaping immune cell development. Here, we identify a colonic *Wnt4*-expressing stromal cell, enriched during early-life, that promotes iNKT cell proliferation via BMP-MAPK signaling. These stromal cells are spatially associated with iNKT cells and macrophages and exhibit high *Bmp2* expression during the neonatal period. Depletion of BMP2 in *Wnt4*$^{+}$ stromal cells during, but not after, this time window leads to long-lasting reductions in iNKT cells. These stromal cells are shaped by microbial signals, as germ-free and early-life antibiotic-treated mice exhibit increased *Wnt4*$^{+}$ stromal cell abundance and elevated *Bmp2* expression, with excessive iNKT cell accumulation that lasts into adulthood. These persistent changes in iNKT cells due to early-life perturbations are associated with altered susceptibility to later-life mucosal disorders. Importantly, similar stromal cells are present in fetal and neonatal human colon, and human rBMP2 promotes iNKT cell growth. Together, our findings reveal a neonatal colonic stromal niche, orchestrated by microbial cues, that regulates colonic immune homeostasis in later-life.

Introduction

Commensal bacteria colonize the intestinal surface during early-life, a critical period when various immune cell populations infiltrate, establish residency, and differentiate within tissues[1]. This immediate postnatal period represents a pivotal phase during which interactions between microbial-derived signals and host cells profoundly shape the maturation of the intestinal immune system and thus establish a set-point for the composition and function of host responses to external stimuli[2,3]. These activities are especially prominent within barrier surfaces where the immune system and microbiota are in close apposition. Further, such events are encompassed within the “hygiene hypothesis” that has proposed early-life microbial exposures may determine later-life susceptibility to autoimmune conditions such as asthma and atopy[4]. Consistent with this, several clinical studies have linked childhood antibiotic use to an elevated risk of developing inflammatory bowel disease (IBD) later in life[5-8]. However, the underlying mechanisms of how early-life microbiota influences the intestinal immune system and its long-term consequences, remain incompletely understood. Recent investigations have identified several unconventional T cell subsets that infiltrate intestinal tissues during early-life whereupon they establish tissue residency[9]. These cells respond to microbial-derived signals that are temporally restricted to this developmental window, which is essential for establishing their functional homeostasis in the gut[9]. Among these, invariant natural killer T (iNKT) cells have been recognized as one of the key regulators of immune responses and disease susceptibility in later-life[2,10].

iNKT cells are innate-like T lymphocytes that develop within the thymus and subsequently colonize extrathymic tissues such as the spleen, liver, lungs, skin, and intestines where they establish residency[11-13]. A major class of iNKT cells express a semi-invariant T cell receptor (Vα14-Jα18 in mice and Vα24-Jα18 in humans), which recognize endogenous and exogenous lipid antigens presented by the non-classical major histocompatibility complex (MHC) class I molecule-CD1d[14]. These cells can be identified based upon the binding of their T cell receptor (TCR) to a specific lipid (α-galactosylceramide or αGalCer)-in the context of CD1d[15,16]. iNKT cells respond rapidly to immune activation and serve as potent sources of various cytokines and chemokines[17]. In human IBD patients, iNKT cells within the intestinal lamina propria (LP) produce proinflammatory cytokines such as TNF, IFNγ, IL-17A and IL-13, which can disrupt epithelial barrier integrity and contribute to disease pathology[18]. In a murine model of ulcerative colitis, iNKT cells mediate inflammation in response to oxazolone, a compound that possesses a structure that is contained within various microbial, dietary, and industrial sources[19]. Consistent with this, mice deficient in CD1d or Jα18, which lack iNKT cells, exhibit attenuated inflammation in the oxazolone-induced colitis model[20]. Our recent studies in murine models have demonstrated that the absence of commensal microbiota during the first two weeks of life, but not thereafter, leads to an increased accumulation of colonic iNKT cells that persists into adulthood, resulting in heightened susceptibility to oxazolone-induced colitis[10,21]. Additionally, the human commensal bacterial species *Bacteroides fragilis* produces

inhibitory lipid antigens that restrain iNKT cell proliferation during early life[21,22]. The early-life microbiota regulates the abundance of embryonic-derived colonic macrophages, whose depletion before postnatal day 12, but not later, impairs iNKT cell accumulation and protects against colitis in adult mice[12]. These findings suggest that microbial cues and tissue-resident macrophages cooperate during a critical developmental window to establish a colonic iNKT cell niche. However, the cellular and molecular circuits through which colonic tissue niches modulate iNKT cell programming during early life remain poorly defined, limiting the development of targeted immunomodulatory strategies.

Transcriptomic profiling of early-life colonic macrophages has revealed signatures suggestive of interactions with mesenchymal cells[12]. Consistent with this, emerging evidence implicates mesenchymal stromal cells as key regulators of barrier tissue homeostasis during early-life. In gut-draining mesenteric lymph nodes (mLN), neonatal microbial exposure durably imprints the stromal compartment, thereby modulating the capacity of resident dendritic cells to induce immune tolerance[23]. In the skin, neonatal inflammation induces the accumulation of subcutaneous fibroblasts that interact with and promote type 2 helper T cells which influences wound repair responses later in life[24]. In the small intestine, neonatal lymphotoxin beta receptor (LTβR)-positive stromal cells in the lamina propria (LP) villi regulate epithelial maturation and $CD103^{+}CD11b^{+}$ DCs in the LP and mLN, impacting postnatal tissue growth and injury repair[25]. However, a comprehensive classification and understanding of the roles of intestinal LP stromal cells

during early development remains incomplete. Specifically, the contribution of defined early-life stromal cell subsets to the programming of tissue-resident lymphocytes, including iNKT cells, remains largely unexplored.

Here, we identify a previously uncharacterized population of *Wnt4*-expressing stromal cells enriched in the early-life colonic lamina propria that collaborates with macrophages to establish a tissue niche supporting iNKT cell homeostasis. These stromal cells drive iNKT cell proliferation via BMP2-MAPK signaling during a critical postnatal window, thereby imprinting the long-term residency and functional potential of colonic iNKT cells. The presence of a similar stromal cell population in fetal and neonatal human colon suggests that this niche may represent a conserved early-life mechanism regulating mucosal immune development. These findings highlight a potential opportunity to modulate stromal cell-mediated signals during early life to influence disease susceptibility later in life.

Results

Identification of a Unique *Wnt4*$^{+}$ Colonic Stromal Population in Mice that is Regulated by Macrophages During Early-Life

Our previous work demonstrated that embryonic macrophages imprint iNKT cell levels during early-life[12]. However, the cellular and molecular mechanisms underlying this process remained undefined. To investigate how embryonic macrophages regulate

colonic iNKT cells, we performed single-cell RNA sequencing (scRNA-seq) on control (CT: *LysCre*$^{+/-}$, *Csf1r*$^{DTR-/-}$) and embryonic macrophage-depleted (MM^{DTR}: *LysCre*$^{+/-}$, *Csf1r*$^{DTR+/-}$) mouse colon LP cells at postnatal Day 9, as previously described[12]. This analysis aimed to identify the most dysregulated cell populations in the colon LP following diphtheria toxin (DT)-mediated macrophage depletion between Day 6 and Day 8 of life as previously performed[12] (Supplementary Fig. 1a). After quality control, we analyzed 4,982 cells from CT mice (n = 3) and 4,672 cells from MM^{DTR} mice (n = 3). Cell populations were visualized using uniform manifold approximation and projection (UMAP) (Fig. 1a). We identified 16 distinct cell clusters in the Day 9 colon LP based on their characteristic gene expression profiles (Fig. 1a; Supplementary Data 1). These included four immune cell clusters (C9: innate lymphoid cells, C10: dendritic cells, C13: macrophages/neutrophils, and C14: T cells); a glial cell cluster (C7) expressing *Foxd3* (Forkhead Box D3) and *Ptprz1* (Protein Tyrosine Phosphatase, Receptor Type Z1); a pericyte cluster (C12) expressing *Pdgfrb* (Platelet-Derived Growth Factor Receptor Beta) and *Cox4i2* (Cytochrome C Oxidase Subunit 4 Isoform 2); and an endothelial cell cluster (C15) expressing *Pecam1* (Platelet and Endothelial Cell Adhesion Molecule 1) and *Cdh5* (Cadherin 5) (Supplementary Fig. 1b, c). The remaining nine clusters comprised mesenchymal stromal cells expressing *Pdgfra* (Platelet-Derived Growth Factor Receptor Alpha), *Ptch1* (Patched 1), *Lum* (Lumican), and *Col16a1* (Collagen Type XVI Alpha 1) (Supplementary Fig. 1b). Among these, C4 was identified as a proliferating cell population expressing *Mki67* (Marker of Proliferation Ki-67) and *Cdk1* (Cyclin-Dependent Kinase 1),

while C11 represented smooth musclse cells expressing *Lmod1* (Leiomodin 1) and *Cnn1* (Calponin 1). The remaining six mesenchymal stromal cell clusters (C0, C1, C2, C3, C5, C6, C8) were classified based on their unique marker genes (Fig. 1a; Supplementary Fig. 1c).

To determine which cluster exhibited the most significant dysregulation following embryonic macrophage depletion, we performed differentially expressed gene (DEG) analysis between CT and MM^{DTR} for each cluster. Most clusters showed minimal changes, with fewer than ten DEGs that reached significance (P_{adj}<0.05, log_2|FC|>1), except for C13 (macrophages/neutrophils) and C1 (*Wnt4*$^+$ stromal cells) (Supplementary Fig. 1d; Supplementary Data 2). Further sub-clustering of C13 revealed two distinct populations: macrophages expressing *Adgre1* (Adhesion G Protein-Coupled Receptor E1, also known as F4/80), *Fcgr1* (Fc Gamma Receptor 1, also known as CD64), and *Cx3cr1* (C-X3-C Motif Chemokine Receptor 1), and neutrophils expressing *Csf3r* (Colony Stimulating Factor 3 Receptor, also known as G-CSF receptor), *S100a8* (S100 Calcium Binding Protein A8), and *S100a9* (S100 Calcium Binding Protein A9) (Supplementary Fig. 1e, f). Notably, macrophage abundance significantly decreased in MM^{DTR} mice, while neutrophil infiltration increased in MM^{DTR} compared with CT mice (Supplementary Fig. 1e, g). This was further confirmed by the DEGs of all colon LP cells between CT and MM^{DTR} mice **(**Supplementary Fig. 1h; Supplementary Data 3), confirming that DT efficiently induces colon embryonic macrophage cell death, which may lead to secondary neutrophil

infiltration[12]. Beyond macrophage depletion, the most significantly dysregulated cell population was the C1 *Wnt4*$^{+}$ stromal cell cluster (Supplementary Fig. 1d). This cluster also exhibited the most pronounced reduction in cell abundance following macrophage depletion (Fig. 1b), with a 30% decrease in MM^{DTR} compared to CT mice (Supplementary Data 1). Notably, *Wnt4*, *Adamdec1* (ADAM-like decysin 1, a metalloproteinase), and *Agt* (Angiotensinogen) were the top three feature genes of this population, which were also enriched in the C8 *Fgf9*$^{+}$ stromal cluster (Fig. 1c; Supplementary Fig. 1c).

Guided by these scRNA-seq gene expression profiles, we developed a flow cytometry gating strategy to distinguish and enumerate colonic stromal cell populations through cell surface antibody staining. At postnatal Day 9, nearly all colonic stromal cells expressed *Pdgfra* (CD140a) and *Ncam1* (CD56) (Fig. 1d). However, *Wnt4*$^{+}$ (cluster 1) and *Fgf9*$^{+}$ (cluster 8) stromal cells uniquely lacked *Cd9* and *Cd34*, distinguishing them from other stromal populations (Fig. 1d). Based on these surface markers, we defined *Wnt4*$^{+}$ and *Fgf9*$^{+}$ stromal cells as Lin^{-}NCAM1^{+}CD9^{-}CD34^{-} (named as P1) and all other stromal cells as Lin^{-}NCAM1^{+}CD9^{+}CD34^{+} (named as P2) using fluorescence-activated cell sorting (FACS) (Fig. 1e; Supplementary Fig. 2a). We further confirmed the identity of P1 and P2 populations after flow-cytometry directed purification through quantitative reverse transcription PCR (qRT-PCR), which showed that both expressed typical stromal markers *Lum*, *Pdgfra*, and *Col6a1* (Supplementary Fig. 2b). However, transcript levels of *Wnt4*, *Adamdec1*, and *Agt* (enriched in *Wnt4*$^{+}$ and *Fgf9*$^{+}$ stromal cells) were

significantly higher in P1 cells compared to P2 cells (Fig. 1f). These results validate our flow cytometry-based method for defining *Wnt4*$^{+}$ stromal cells, as identified by scRNA-seq.

To further confirm the reduction of P1 cells following embryonic macrophage depletion as observed in scRNA-seq (Fig. 1b), we performed flow cytometry analysis on Day 9 colonic LP cells from CT and MM^{DTR} mice after administering DT from Day 6 to Day 8 after birth (Supplementary Fig. 1a). Consistent with our transcriptomic findings, macrophage, iNKT cell, and P1 stromal cell abundances were significantly reduced in MM^{DTR} mice compared to littermate controls, whereas P2 cell abundance remained unchanged (Fig. 1g, h; Supplementary Fig. 2c). Finally, bulk RNA sequencing of whole colons from Day 9 CT and MM^{DTR} mice following DT-mediated macrophage depletion (Supplementary Fig. 2d) revealed that their transcriptional signatures were distinct based upon principal component analysis (PCA) (Supplementary Fig. 2e) in conjunction with a significant reduction in several stromal cell-related genes that included the P1-specific markers *Adamdec1* and *Agt* (Supplementary Fig. 2f). These results are consistent with our scRNA-seq and flow cytometry data, further supporting the significant reduction in abundance of *Wnt4*$^{+}$ (P1) stromal cells and iNKT cells in MM^{DTR} mice after embryonic macrophage depletion. Collectively, these findings demonstrate that depletion of embryonic macrophages results in a marked reduction of a distinct *Wnt4*$^{+}$ colonic stromal population (P1). These data further allowed us to hypothesize that embryonic

macrophages and *Wnt4*$^{+}$ stromal cells cooperatively establish a tissue niche that may deliver regulatory cues to colonic iNKT cells during early-life.

P1 Stromal Cells Are Enriched in the Early-Life Mouse Colon and Support iNKT Cell Proliferation *Ex Vivo*

Mesenchymal stromal cells in the gut are known to secrete factors such as WNTs and bone morphogenetic proteins (BMPs) to regulate the balance between proliferation and differentiation of intestinal stem cells and epithelial cells during homeostasis and tissue repair in adult life[26-28]. Additionally, they may influence intestinal immune populations through direct cell-cell interactions via adhesion molecules and the secretion of cytokines and chemokines, including IL-6, CCL2, and CCL5.[29-31]. However, little is known about the role of colonic stromal cells in immune cell regulation during early-life, their specific characteristics or the types of immune cells with which they interact. To investigate whether P1 stromal cells can directly regulate iNKT cells, we developed an ex vivo stromal-T cell co-culture assay (Supplementary Fig. 3a). We first isolated 20,000 P1 and P2 stromal cells by FACS from the Day 9 mouse colon and maintained them in RPMI complete culture medium in 96-well plates. We observed that primary isolated early-life colon stromal cells survived for 4-5 days *ex vivo*. Both P1 and P2 began to elongate after 24 hours in culture and formed a stromal cell layer with distinct morphology by 96 hours (Fig. 2a). Due to the very low abundance of endogenous colonic iNKT cells, we isolated pan T cells (including iNKT cells) from the adult thymus and added 100,000 T cells to P1

and P2 stromal cells followed by co-culture for an additional three days (Supplementary Fig. 3a, b). Flow cytometric analysis revealed that while both P1 and P2 stromal cells maintained higher levels of CD1d-tetramer-positive iNKT cells compared to the control which lacked stromal cells (Fig. 2b). However, only P1 stromal cells promoted iNKT cell proliferation, as indicated by increased Ki67 expression (Fig. 2c). In contrast, P2 stromal cells only increased overall thymic cell survival rates without promoting iNKT cell proliferation (Fig. 2c, d).

Given that the critical "window of opportunity" for colonic iNKT cell development occurs between Days 6 and 12 after birth[10,12], we examined iNKT cell proliferation *in vivo* at different neonatal stages, both within (Day 9) and outside (Days 15 and 20) this window. At Day 9, approximately 60% of colonic iNKT cells were $Ki67^{+}$ proliferating cells; this percentage decreased to 30% at Day 15 and was even lower at Day 20. In contrast, splenic iNKT cells showed no significant proliferation differences across these developmental stages (Fig. 2e). This suggests that P1 stromal cells may regulate colonic iNKT cell proliferation in a "window-specific" manner *in vivo*. To test this hypothesis, we used flow cytometry to track the abundance of P1 and P2 stromal cells in the colon LP from Day 5 to Day 20. Interestingly, P1 cells were highly enriched during the iNKT cell developmental window (Day 5-9) but significantly declined after Day 10, whereas P2 cells gradually increased from Days 5 to 20 (Fig. 2f). This dynamic change in P1 abundance parallels that of embryonic macrophages and aligns with the "window of opportunity"

when colonic iNKT cells are regulated[10,12,21]. To further confirm the enrichment of the P1 subset during early-life, we performed qRT-PCR analysis of whole-colon samples and found that the expression of the P1-specific marker *Wnt4* progressively decreased at Day 15 and 12 weeks compared to Day 9 of postnatal life (Supplementary Fig. 3c). Additionally, we integrated scRNA-seq data from Day 9 colon lamina propria cells (Fig. 1a) with a published adult healthy wild-type mouse dataset[32] (Fig. 2g; Supplementary Fig. 3d). UMAP analysis identified 15 cell populations based on their feature genes (Supplementary Data 4), with clusters 0, 1, 2, 3, 4, 7, and 8 corresponding to mesenchymal stromal cells expressing *Pdgfra, Ptch1, Lum, Dcn,* and *Col6a1* (Supplementary Fig. 3e). Among these stromal cells, cluster 4 expressed high levels of the P1-specific markers *Wnt4* and *Agt* (Fig. 2h), which were significantly enriched in Day 9 colons (21.7% of total stromal cells) compared to adults (3.1% of total stromal cells) (Fig. 2i).

Since P1 stromal cells are enriched at Day 9 and decline significantly by Day 15, we next examined whether colon P1 cells at different developmental stages (within and outside the "window") regulate iNKT cell proliferation differently. We isolated P1 and P2 stromal cells from Day 9 and Day 15 colons (Supplementary Fig. 3f, g) and co-cultured them with thymic T cells for three days. Consistent with our hypothesis, Day 9 P1 stromal cells most effectively supported iNKT cell numbers (Fig. 2j) and proliferation (Fig. 2k) *in vitro* compared to Day 15 P1 cells, without affecting the overall thymic cell survival

(Supplementary Fig. 3h). In contrast, P2 cells from Day 9 and Day 15 displayed comparable abilities to support iNKT cell proliferation and survival (Supplementary Fig. 3i, j). Taken together, these data demonstrate that colonic *Wnt4*$^+$ (P1) stromal cells are highly enriched during early-life and play a crucial role in supporting iNKT cell proliferation within the developmental "window of opportunity."

Early-Life P1 Stromal Cells Regulate iNKT Cell Proliferation Through BMP-MAPK Signaling

To identify molecules enriched in Day 9 P1 stromal cells that target iNKT cells, we performed bulk RNA sequencing (RNA-seq) on FACS-sorted early-life Day 9 P1 and P2, as well as later-life Day 15 P1 and P2 from the WT mouse colon. Differentially expressed gene (DEG) analysis (P_{adj}<0.05, $\log_2$|FC|>1) between Day 9 P1 and Day 9 P2 (Supplementary Data 5) confirmed that C1 *Wnt4*$^+$ stromal cell-specific marker genes, including *Wnt4, Agt,* and *Adamdec1* (Fig. 1c), were significantly upregulated in Day 9 P1, whereas other stromal cell feature genes (Supplementary Fig. 1c), such as *Igfbp6* (Insulin-like growth factor binding protein 6)*, Cmah* (Cytidine monophosphate-N-acetylneuraminic acid hydroxylase)*, Efemp1* (EGF-containing fibulin-like extracellular matrix protein 1), and *Igf2* (Insulin-like growth factor 2), were enriched in Day 9 P2 cells (Supplementary Fig. 4a). Furthermore, all the top 20 feature genes of C1 *Wnt4*$^+$ stromal cells (Supplementary Data 1) were specifically enriched in both Day 9 and Day 15 P1 samples compared to P2 (Supplementary Fig. 4b). Gene Ontology (GO) analysis

revealed distinct functional profiles between these populations: Day 9 P1 cells were enriched in pathways related to "vasculature development," "regulation of cell migration/adhesion," and "tyrosine kinase signaling pathway" (Supplementary Fig. 4c), whereas Day 9 P2 cells showed enrichment in pathways related to "regulation of epithelial cell proliferation," "response to growth factor stimulus," and "response to wounding" (Supplementary Fig. 4d). These findings suggest that P1 and P2 represent phenotypically and functionally distinct stromal populations in the early-life colon and further validate our FACS gating strategy (Fig. 1e) for distinguishing C1 *Wnt4*$^{+}$ stromal cells identified via scRNA-seq.

Principal component analysis revealed that Day 9 P1 and Day 15 P1 samples formed distinct clusters, whereas Day 9 P2 and Day 15 P2 samples clustered together (Fig. 3a). This suggests that in addition to the dynamic changes in P1 cell abundance, its gene expression program also undergoes substantial changes during early-life. The extent of transcriptional changes was supported by the number of significant DEGs between Day 9 P1 and Day 15 P1 (1,220 DEGs, Supplementary Fig. 4e) and between Day 9 P2 and Day 15 P2 (481 DEGs, Supplementary Fig. 4f). As previously described, Day 9 P1 cells exhibited an increased ability to support iNKT cell proliferation *in vitro* relative to P2 cells (Fig. 2c, k). To further investigate the molecular mechanisms underlying these differences, we intersected the DEGs from Day 9 P1 vs. Day 15 P1 with those from Day 9 P2 vs. Day 15 P2, identifying 1,052 genes that were uniquely dysregulated in P1 cells between early-

and later-life (Supplementary Fig. 4g). GO analysis of the significantly dysregulated genes (Supplementary Data 6) with high expression levels (P_{adj}<0.05, $\log_2$|FC|>1, avgTPM>10) revealed that genes upregulated in Day 15 P1 were predominantly associated with mitochondrial functions (Fig. 3b). In contrast, genes upregulated in Day 9 P1 were enriched in an intriguing pathway characterized as "positive regulation of MAPK cascade" (Fig. 3c), which is directly linked to regulation of cell proliferation[33]. Interestingly, among all the genes identified in this pathway, *Bmp2* (Bone Morphogenetic Protein 2) was the only one that was significantly upregulated in Day 9 P1 (clusters 1 and 8) compared not only with Day 15 P1 cells but also with Day 9 P2 cells (Fig. 3d, e). BMP signaling has been reported to regulate cell proliferation by activating the noncanonical MAPK pathway[34]. Activation of MAPK (ERK1/2, p38, JNK1/2) is the noncanonical signaling pathway downstream of BMP-associated signaling, which modulates several cellular processes, including proliferation, migration, and differentiation[35-37]. These findings suggest that early-life P1 stromal cells might regulate colonic iNKT cell proliferation through BMP2 production.

To further investigate this hypothesis, we sorted colonic iNKT cells and conventional TCR-αβ T (αβT) cells from Day 9 mouse colon and performed bulk RNA-seq, which were distinct based upon PCA (Supplementary Fig. 4h). As expected, genes upregulated in αβT cells were associated with conventional T cell functions, such as "T cell proliferation," "T cell energy," and "alpha-beta T cell activation" (Supplementary Fig. 4i). Conversely,

iNKT cells exhibited upregulation of genes associated with cytotoxicity and high proliferative potential, including *Gzma* (Granzyme A)*, Gzmb* (Granzyme B)*, Tnf* (Tumor necrosis factor), and *Mki67* (Supplementary Fig. 4j; Supplementary Data 7). Importantly, Day 9 iNKT cells also exhibited upregulation of genes associated with the "MAPK signaling pathway" (Fig. 3f), including *Map2k3* (Mitogen-activated protein kinase kinase 3)*, Myc, Rps6ka1* (Ribosomal protein S6 kinase A1)*, Dusp1* (Dual specificity phosphatase 1)*, Lamtor3* (Late endosomal/lysosomal adaptor, MAPK and MTOR activator 3), and *Nr4a1* (Nuclear receptor subfamily 4 group A member 1) (Fig. 3g). Additionally, BMP receptor genes *Bmpr2* (Bone morphogenetic protein receptor type 2) and *Acvr2a* (Activin A receptor type 2A) were upregulated in Day 9 iNKT cells compared to αβT cells (Fig. 3g), suggesting that early-life P1 stromal cells regulate iNKT cell proliferation through the BMP2-BMPR axis by activating MAPK signaling. To validate this mechanism, we sorted Day 9 iNKT cells from both control (CT) and Day 6-8 macrophage-depleted (MM^{DTR}) mouse colons. Notably, genes significantly downregulated in iNKT cells from MM^{DTR} colons were enriched in "MAPK signaling pathway" GO terms (Supplementary Fig. 4k-m; Supplementary Data 8). This indicates that embryonic macrophage depletion reduces the abundance of P1 stromal cell, the main producer of *Bmp2* in early-life colon (Fig. 3e), together with decreased MAPK pathway activation and proliferation of iNKT cell.

Next, we assessed BMP receptor protein expression on Day 9 and Day 15 colonic αβT and iNKT cells via flow cytometry. Consistent with transcriptome data (Fig. 3g), Day 9

iNKT cells exhibited significantly higher expression levels of BMPR1A, BMPR1B, and BMPR2 compared to αβT cells and Day 15 iNKT cells (Fig. 3h; Supplementary Fig. 5a). These data suggest that P1 cell induction of MAPK pathway activation and iNKT cell proliferation is due to BMP2 signaling within the “window of opportunity”. To investigate this, we cultured thymic T cells in the presence of recombinant mouse BMP2 at different concentrations (0, 50, 100 ng/ml) for three days. Both CD1d-tetramer positive iNKT cell abundance and its Ki67 mean fluorescence intensity (MFI) increased in a BMP2 dose-dependent manner (Fig. 3i; Supplementary Fig. 5b), demonstrating that BMP2 is sufficient to induce iNKT cell proliferation *in vitro*. To further determine whether P1 stromal cells promote iNKT cell proliferation via BMP signaling, we added the BMP type I receptor inhibitor Dorsomorphin[38] (10 μM) to the Day 9 P1 stromal-T cell co-culture for three days, and observed that iNKT cell number and proliferation were significantly reduced compared to vehicle-treated samples (Fig. 3j; Supplementary Fig. 5c). Consistent with this, intraperitoneal (IP) injection of Dorsomorphin (10μg/gram body weight) into WT mice from Days 6-12 of postnatal life (the "window of opportunity" when P1 stromal cells are most abundant and express higher BMP2 levels) significantly reduced iNKT cell levels and proliferation rates in the colon at Day 13, whereas αβT cells remained unaffected (Fig. 3k; Supplementary Fig. 5d). In contrast, Dorsomorphin injection outside the "window of opportunity" (Days 16-22) had no effect on iNKT or αβT cell populations (Fig. 3l; Supplementary Fig. 5e). Together, these findings indicate that P1 stromal cells upregulate BMP2 expression during early-life, which acts on BMP receptors specifically expressed

on iNKT cells. This, in turn, activates noncanonical BMP-MAPK signaling, promoting iNKT cell proliferation.

Macrophages and P1 Stromal Cells Form a Tissue Niche for Colonic iNKT Cells in Early-Life

While the *in vitro* co-culture system of colonic stromal cells and thymic T cells provides insights into cellular interactions, it does not provide insights into the anatomical localization of these cells *in situ*. Colonic iNKT cells are tissue-resident immune cells that colonize the intestine during the early postnatal period[12]. Consistent with this, genes associated with integrin-mediated cell adhesion are significantly upregulated in iNKT cells compared to conventional αβT cells (Fig. 3f, g), suggesting the presence of a specialized tissue niche that supports iNKT cell maintenance in the early-life colon. Given that embryonic macrophages upregulate genes associated with extracellular matrix (ECM) formation at Day 8[12] and that their depletion leads to a remarkable reduction in P1 stromal cells (Fig. 1b), we hypothesized that macrophages are closely associated with P1 stromal cells and that both contribute to a structural niche for iNKT cells during early-life.

To define the spatial localization of macrophages, iNKT cells, and P1 stromal cells, we performed immunofluorescence (IF) staining. Bulk RNA-seq analysis of Day 9 P1 and P2 stromal cells revealed that *Pdgfra* is a highly expressed pan-stromal marker that marks both P1 and P2 populations. In contrast, *Wnt4*, a hallmark of P1 cells, was expressed at

barely detectable levels in P2 cells (Supplementary Fig. 6a). Although *Wnt4* is a feature gene of P1 stromal cells compared to P2 cells (Fig 1c, d), the *Wnt4* expression levels are low in P1 cells (avgTPM<1) (Supplementary Fig. 6a). Consistent with this, when we examined *Wnt4-eGFP-CreER^{T2}* mice[39], we found negligible eGFP signals in colon stromal cells by flow cytometry (Supplementary Fig. 6b), ruling out this model as a viable tool for *in vivo* P1 cell labeling. Interestingly, we identified *Foxl1* (Forkhead box L1) as a gene specifically expressed in Day 9 and Day 15 P1 stromal cells but absent in P2 (Fig. 4a, b; Supplementary Fig. 6c). Thus, we applied flow cytometry gating method to analyze the Day 9 colon tdTomato$^+$ cells of the *Foxl1-CreER^{T2}-tdTomato* mice[40] (Supplementary Fig. 6d). This confirmed that approximately 80% of all tdTomato$^+$ stromal cells were CD9$^-$ CD34$^-$ P1 stromal cells (Fig. 4c), while nearly 50% of all CD9$^-$CD34$^-$ P1 stromal cells were tdTomato$^+$ (Fig. 4d), validating this model as a highly specific and efficient tool for marking P1 stromal cells *in vivo*. Using *Foxl1-CreER^{T2}-tdTomato* mice, we examined the localization of P1 and P2 stromal cells in cross-sections of the Day 9 colon. IF staining for tdTomato (P1) and PDGFRA (all stromal cells) demonstrated that tdTomato$^+$PDGFRA$^+$ (P1) stromal cells were confined to the lamina propria of the mucosa, whereas tdTomato$^-$PDGFRA$^+$ (P2) stromal cells were predominantly located in the submucosal muscularis layer (Fig. 4e). These findings further establish P1 as a unique early-life stromal population that is morphologically (Fig. 2a), anatomically (Fig. 4e), and functionally (Supplementary Fig. 4c, d) distinct from other stromal cells.

Due to the lack of specific protein markers that can accurately distinguish colonic iNKT cells from conventional αβT cells, direct *in situ* CD1d-tetramer staining presents a technical challenge, particularly given the high background signal in intestinal tissue and the low abundance of colonic iNKT cells (~300 cells per whole Day 9 colon). To overcome this, we employed the adoptive thymic iNKT cell transfer method as an alternative approach[12]. Thymic cells from CD45.1 mice were first stained with PE-conjugated CD1d-tetramer, enriched using MACS beads (~60% purity), and subsequently sorted by FACS (~97% purity) (Fig. 4f; Supplementary Fig. 6e). These purified CD45.1$^+$ iNKT cells were transferred intraperitoneally into CD45.2 WT recipient mice at Day 4 (a time point when thymic iNKT cells begin to colonize the colon) (Fig. 4f). Flow cytometry at Day 10 confirmed that no CD45.1$^+$ cells were detected in non-transferred control mice, whereas nearly all CD45.1$^+$ cells (~95%) in recipient colons were CD1d-tetramer$^+$ iNKT cells (Supplementary Fig. 6f). Immunofluorescence (IF) staining of CD45.1 expressing cells (that represent the iNKT cells) in recipient colons at Day 10 revealed that they were exclusively localized within the LP (Fig. 4g), coinciding with the anatomical location of P1 stromal cells and spatially separated from P2 cells that localize to submucosal regions of the gut (Fig. 4e). To further explore the cellular composition of early-life colonic iNKT cell niche, we crossed *Foxl1-CreER^{T2}-tdTomato* mice with *Cx3cr1-GFP* mice[41], in which GFP labels colonic macrophages, generating double reporter mice as recipients for purified CD45.1$^+$ iNKT cell transfer (Fig. 4f). Triple IF staining for tdTomato (P1 stromal cells), GFP (macrophages), and CD45.1 (iNKT cells) revealed a structured niche within the

crypts, where macrophages and P1 stromal cells surrounded 80% of total CD45.1$^+$ colonic iNKT cells at Day 10 after birth (Fig. 4h, i). These findings support the concept that P1 stromal cells, but not other stromal populations, play a critical role in establishing a tissue niche that supports colonic iNKT cells within the early-life “window of opportunity”.

Early-Life, but Not Later-Life, P1 Stromal Cell-Specific Depletion of BMP2 Prevents Long-Term Colonic iNKT Cell Accumulation

While our findings have demonstrated that inhibition of BMP signaling via IP injection of Dorsomorphin during early life results in decreased proliferation and abundance of colonic iNKT cells (Fig. 3k), Dorsomorphin is a broad inhibitor of BMP receptors. It is not specific to BMP2 derived from P1 stromal cells and may also impact other pathways, such as mTOR and AMPK signaling[38]. To address this limitation, we generated *Foxl1-CreER^{T2}-tdTomato*; *Bmp2$^{fl/fl}$* (*Foxl1^{CreER}Bmp2$^{fl/fl}$*) mice[42], in which *Bmp2* is specifically deleted in *Foxl1*-expressing P1 stromal cells following tamoxifen (TAM) administration. Using this model, we administered TAM (50μg/gram body weight) every other day from postnatal Day 6 to Day 12 and collected tissue on Day 13 (TAM6-12 H13, Fig. 5a). This regimen resulted in a significant reduction of *Bmp2* expression in P1, but not in P2, cells in *Foxl1^{CreER+}Bmp2$^{fl/fl}$* mice compared to littermate controls (*Foxl1^{CreER-}Bmp2$^{fl/fl}$*) at Day 13 without affecting *Wnt4* expression (Supplementary Fig. 7a). Remarkably, the depletion of BMP2 in P1 stromal cells during this early-life "window of opportunity" led to a significant decrease in iNKT cell numbers across different colonic regions (Fig. 5b; Supplementary

Fig. 7b), without affecting iNKT cell proliferation or abundance in the spleen or thymus (Supplementary Fig. 7c). This effect was specific to colonic iNKT cells, as no changes were observed in other cell types, including P1 and P2 stromal cells, macrophages, or conventional αβT cells, within the colonic lamina propria (LP) (Fig. 5c; Supplementary Fig. 7d).

Although colonic iNKT cell numbers were reduced at Day 13 following P1-specific BMP2 depletion from Day 6-12, no significant differences in iNKT cell proliferation were observed at this time point (Fig. 5b). This finding is consistent with our previous observations that although P1 cell levels and iNKT cell proliferation rates peak at Day 9 and decline thereafter, the consequence of these activities is a later increase in iNKT cell levels (Fig. 2e, f). To further address this issue and confirm the direct role of P1-derived BMP2 in promoting colonic iNKT cell proliferation *in vivo*, we administered TAM every other day from Day 6 to Day 8 and analyzed the tissue at Day 9 (TAM6-8 H9, Fig. 5d). We observed that P1-specific BMP2 depletion during this early-life period was sufficient to reduce both the proliferation and abundance of colonic iNKT cells in *Foxl1*$^{CreER+}$*Bmp2*$^{fl/fl}$ mice compared to controls (Fig. 5e), while having no impact on iNKT cells in the spleen or thymus or on other colonic immune cell populations (Supplementary Fig. 7e, f). To further validate these findings, we generated another genetic mouse model (*Pdgfra*$^{CreER+}$*Bmp2*$^{fl/fl}$)[43], in which *Bmp2* is depleted across all stromal cell populations following TAM administration. Indeed, *Bmp2*, but not *Wnt4*, expression was significantly

reduced in both P1 and P2 stromal cells at Day 9 after TAM injection from Day 6-8 (Supplementary Fig. 7g). In accordance with our observations in *Foxl1*^{CreER}*Bmp2*$^{fl/fl}$ mice, this global stromal depletion of BMP2 similarly resulted in decreased colonic iNKT cell proliferation and abundance (Supplementary Fig. 7h) without affecting the abundance of P1 and P2 stromal cells, macrophages, or αβT cells in the colon (Supplementary Fig. 7i) or iNKT cells in the spleen and thymus (Supplementary Fig. 7j). In contrast, administration of TAM to *Foxl1*^{CreER}*Bmp2*$^{fl/fl}$ mice from Day 14 to Day 20 (TAM14-20 H21, Fig.5f), a period outside the "window of opportunity" when P1 stromal cell abundance, *Bmp2* expression, and iNKT cell proliferation rates have already declined, no effect on colonic iNKT cells compared to controls was observed (Fig. 5g). These findings indicate that BMP2 derived from P1 stromal cells regulates colonic iNKT cells only within the first two weeks of life, aligning with the previously described "window of opportunity" associated with microbiota and macrophage-iNKT cell regulation[10,12].

To investigate whether early-life depletion of BMP2 in P1 stromal cells has long-term consequences, we administered TAM to *Foxl1*^{CreER}*Bmp2*$^{fl/fl}$ mice from Day 6-12 and maintained them until Day 56 (TAM6-12 H56, Fig. 5h). Although iNKT cell proliferation rates were low and unchanged in TAM-treated *Foxl1*^{CreER} negative and positive adult mice, iNKT cell abundance across all colonic regions remained significantly reduced in *Foxl1*$^{CreER+}$*Bmp2*$^{fl/fl}$ mice compared to controls (Fig. 5i; Supplementary Fig. 7k). Like the observations in the mice that were examined in early-life (Supplementary Fig. 7c), there

were no differences in adult iNKT cells of spleen or thymus that were subjected to TAM treatment (Supplementary Fig. 7l). This long-term effect was specific to colonic iNKT cells, as other immune cell populations, including αβT cell subtypes, B cells, macrophages, dendritic cells, and innate lymphoid cells (ILCs), remained unchanged in the adult colon (Supplementary Fig. 7m).

Finally, we explored whether the persistent reduction in distal colonic iNKT cells (Supplementary Fig. 7k) due to early-life BMP2 depletion influences susceptibility to iNKT cell-mediated diseases in adulthood. Oxazolone-induced colitis is a well-established colitis model that depends on colonic iNKT cell levels[20]. Given that oxazole compounds from microbes and diet activate AhR in intestinal epithelial cells (IECs), leading to IEC CD1d-dependent activation of colonic iNKT cells and subsequent intestinal inflammation[19], we tested the impact of early-life P1 stromal-specific BMP2 depletion in this model. *Foxl1*$^{CreER+}$*Bmp2*$^{fl/fl}$ and control mice (*Foxl1*$^{CreER-}$*Bmp2*$^{fl/fl}$) received TAM from Day 6-12 and were exposed to oxazolone or vehicle control via rectal administration on Day 56 (Fig. 5j). Consistent with their reduced colonic iNKT cell levels (Fig. 5i), *Foxl1*$^{CreER+}$*Bmp2*$^{fl/fl}$ mice were protected from oxazolone-induced colitis as shown by their significantly less weight loss (Fig. 5k) and reduced histopathological damage compared to controls (Fig. 5l). Additionally, colonic iNKT cells play a critical role in host defense against pathogens such as *Listeria monocytogenes*[44]. To assess whether early-life P1 stromal specific BMP2 depletion affects host defense, we administered TAM to

Foxl1^{CreER+}*Bmp2*$^{fl/fl}$ and control mice from Day 6-12 and orally infected them with *Listeria monocytogenes*[45] (3 x 10^9 CFU) at Day 56 of life (Fig. 5m). *Foxl1*$^{CreER+}$*Bmp2*$^{fl/fl}$ mice exhibited significantly higher *L. monocytogenes* colony-forming units (CFUs) in the colon, ileum, and mesenteric lymph nodes (mLN) compared to controls (Fig. 5n), which correlates with their reduced colonic iNKT cell levels (Fig. 5i). Similar findings have been reported in *Cd1d*-deficient mice[44], which lack iNKT cells, suggesting that decreased colonic iNKT cell numbers in *Foxl1*$^{CreER+}$*Bmp2*$^{fl/fl}$ mice may increase the susceptibility to infection with pathogens. Together, these results highlight that early-life regulation of colonic iNKT cells by P1 stromal cell-derived BMP2 has a lasting impact on host susceptibility to inflammatory and infectious diseases in later-life.

Stromal CD1d Signaling Is Not Required for Colonic iNKT Cell Development

CD1d is essential for thymic iNKT cell selection and maturation; however, its role in peripheral iNKT cell maintenance remains poorly understood with some studies observing it is dispensable[46-48]. Since P1 stromal cells form a tissue niche that is in close proximity to colonic iNKT cells (Fig. 4h) and *Cd1d1* transcripts are detectable in all stromal populations during early-life (Supplementary Fig. 8a, b), we hypothesized that colonic stromal cells might influence iNKT cells not only through BMP2 but also via CD1d-dependent antigen presentation. We consistently observed that the cell surface expression of CD1d was higher and displayed on a greater proportion of colonic P1 and P2 stromal cells compared to CD45$^+$ immune cells in Day 9 WT mice (Supplementary Fig.

8c, d). To investigate whether stromal-specific CD1d expression is necessary for colonic iNKT cell development, we generated *Pdgfra*^{Cre}*Cd1d*$^{fl/fl}$ mice[49]. In *Pdgfra*$^{Cre+}$*Cd1d*$^{fl/fl}$ mice, both the percentage of CD1d^{+} cells and CD1d MFI were significantly reduced in colonic P1 and P2 stromal cells, but not in CD45^{+} immune cells, compared to littermate controls (*Pdgfra*$^{Cre-}$*Cd1d*$^{fl/fl}$) (Supplementary Fig. 8e, f) at Day 13 after birth. However, despite stromal-specific depletion of CD1d, we observed no significant differences in either the abundance or proliferation rate of colonic iNKT cells at Day 13 or Day 56 after birth compared to controls nor the quantity of αβT cells, macrophages, P1 cells and P2 cells (Supplementary Fig. 8g-i). These findings suggest that CD1d-dependent antigen presentation by stromal cells is not required for peripheral colonic iNKT cell maintenance. Alternatively, CD1d expression by other cell types, such as macrophages or intestinal epithelial cells, may compensate for the loss of stromal CD1d, ensuring normal iNKT cell homeostasis.

Absence of Microbiota Increases P1 Stromal Cell Numbers and *Bmp2* Expression in Early-Life, Leading to Excessive Colonic iNKT Cell Accumulation in Adulthood

The microbiota plays a crucial role in regulating epithelial and immune cell homeostasis, including those in the colon[1,50,51]. Our previous studies have shown that the absence of microbiota during early-life, but not after weaning, is associated with increased macrophage cell levels in early-life and long-lasting colonic iNKT cell accumulation that persists into adulthood[10,12]. However, the impact of microbial signals on specific stromal

cell types in early-life colonic development and their relationship with iNKT cells remains unclear. Flow cytometry analysis revealed a significant increase in P1 stromal cell numbers in germ-free (GF) wild-type (WT) mice compared to specific pathogen-free (SPF) WT mice at Day 9 but not at Day 15 after birth (Fig. 6a). No significant differences were observed in P2 stromal cells between GF and SPF mice at these same time-points (Supplementary Fig. 9a). RT-PCR analysis of sorted colonic stromal cells from Day 9 GF and SPF mice showed a significant increase in *Bmp2*, but not *Wnt4*, expression in P1, but not P2, stromal cells in GF mice compared to SPF controls (Fig. 6b). These findings suggest that an absence of microbial signals during early-life promotes colonic iNKT cell accumulation by increasing P1 stromal cell numbers and their BMP2 expression levels, aligning with previous findings showing elevated colonic iNKT cell levels in adult GF mice[10,21]. Given that childhood antibiotic use has been linked to an increased risk of IBD in later life[5-8], it was therefore of interest to investigate whether early-life microbial signals and P1 stromal cell-derived BMP2 also contribute to colonic iNKT cell regulation under germ-reduced conditions. To do so, suckling neonatal WT mice were exposed to broad-spectrum antibiotics (ampicillin trihydrate, gentamicin sulfate, vancomycin hydrochloride) through treatment of their mothers from Day 0 to Day 21 of life. Antibiotic treatment led to a significant increase in P1, but not P2, stromal cell numbers at Day 9 in the pups (Supplementary Fig. 9b). This was accompanied by a higher proliferation rate of colonic, but not thymic or splenic, iNKT cells in antibiotic-treated (Abx) mice compared to SPF controls at Day 9 (Supplementary Fig. 9c, d) and excessive colonic iNKT cell

accumulation at Day 35 (Supplementary Fig. 9e), mirroring observations in GF WT mice on a C57BL/6 background as used here[12].

To further assess whether BMP2 from P1 stromal cells mediates these effects, *Foxl1*^{CreER}*Bmp2*$^{fl/fl}$ mice were treated with antibiotics from Day 0 to Day 21 of life, in conjunction with tamoxifen (TAM) treatment from Day 6 to Day 12 to deplete BMP2 specifically in P1 stromal cells during early life followed by collection of colon tissues in both early-life (Day 9 and Day 13) and adulthood (Day 56) (Fig. 6c). At Day 9, P1 stromal cell numbers and *Bmp2* expression levels were significantly elevated in Abx-treated control mice (Abx *Foxl1*$^{CreER-}$*Bmp2*$^{fl/fl}$) compared to untreated controls (SPF *Foxl1*$^{CreER-}$*Bmp2*$^{fl/fl}$); TAM treatment significantly reduced *Bmp2* expression in both Abx-treated and untreated *Foxl1*$^{CreER+}$*Bmp2*$^{fl/fl}$ mice to a similar level without affecting the elevated quantities of P1 stromal cells caused by Abx treatment (Supplementary Fig. 9f). Notably, colonic iNKT cell proliferation was significantly higher in Abx *Foxl1*$^{CreER-}$*Bmp2*$^{fl/fl}$ mice than in SPF *Foxl1*$^{CreER-}$*Bmp2*$^{fl/fl}$ mice at Day 9, but P1 stromal cell-specific BMP2 depletion (Abx *Foxl1*$^{CreER+}$*Bmp2*$^{fl/fl}$) reduced colonic iNKT cell proliferation to levels comparable to SPF *Foxl1*$^{CreER-}$*Bmp2*$^{fl/fl}$ mice (Fig. 6d). As seen previously (Fig. 5b, e), BMP2 depletion in P1 stromal cells during early-life resulted in a robust reduction in colonic iNKT cell numbers, but not conventional αβT cell, at both Day 9 and Day 13 under both SPF and Abx conditions (Fig. 6e; Supplementary Fig. 9f, g). In addition, we performed early-life adoptive transfer of CD45.1 iNKT cells to track down iNKT cells in the colon and assess

whether the colonic niche structure surrounding iNKT cells is altered under antibiotic treatment or BMP2-deficient conditions which in the latter case was imposed by Dorsomorphin treatment. Notably, we found that neither the overall niche size nor general structural organization of P1 and macrophage was changed compared to the untreated control within or outside the “window of opportunity” (Supplementary Fig. 9h). These results further support our conclusion that embryonic macrophages and P1 stromal cells establish a stable tissue niche for iNKT cells as we continue to observe nests of P1 stromal cells, macrophages and iNKT cells that are displayed as triads of cells. These also suggest that a loss of early-life microbes or BMP2 inhibition alters BMP2 levels and their effects, thereby directly regulating iNKT cell proliferation through BMP receptor signaling without affecting the niche architecture.

At Day 56, *Foxl1*$^{CreER-}$*Bmp2*$^{fl/fl}$ control mice treated with Abx during early-life exhibited increased colonic iNKT cell levels in adulthood compared to SPF controls (Fig. 6f). However, early-life (Day 6-12) depletion of BMP2 in P1 stromal cells (Abx *Foxl1*$^{CreER+}$*Bmp2*$^{fl/fl}$) prevented this abnormal colonic iNKT cell accumulation caused by the absence of early-life microbiota due to antibiotic exposure (Fig. 6f). Next, we examined whether early-life antibiotic exposure and P1 stromal cell specific BMP2 depletion affected iNKT cell differentiation. iNKT cells can be classified into three subsets, NKT1, NKT2, and NKT17, based on transcription factor expression and cytokine production[52]. In early-life (Day 0-21) Abx-treated control mice (Abx *Foxl1*$^{CreER-}$*Bmp2*$^{fl/fl}$),

the excessive colonic iNKT cells at Day 56 were predominantly NKT1 and NKT17 cells compared to untreated controls (Supplementary Fig. 9i). However, early-life (Day 6-12) BMP2 depletion in P1 stromal cells (Abx *Foxl1*$^{CreER+}$*Bmp2*$^{fl/fl}$) significantly reduced NKT1 and NKT17 levels to those of SPF controls (Supplementary Fig. 9i). This suggests that early-life microbial signals and P1 stromal cell-derived BMP2 imprint colonic iNKT cells not only through regulating their cell proliferation and cell accumulation but also by influencing their cell differentiation and function. In association with these persistent cell level changes of adult colonic iNKT cells (Fig. 6f), Abx-treated control mice (Abx *Foxl1*$^{CreER-}$*Bmp2*$^{fl/fl}$) were more susceptible to oxazolone-induced colitis, displaying significant weight loss and increased colon pathology scores compared to untreated SPF controls (SPF *Foxl1*$^{CreER-}$*Bmp2*$^{fl/fl}$) (Fig. 6g-i). However, Abx-treated BMP2-depleted mice (Abx *Foxl1*$^{CreER+}$*Bmp2*$^{fl/fl}$) were protected from this hypersensitivity to oxazolone-induced colitis as shown by comparable weight loss and colon pathology scores in comparison to untreated SPF *Foxl1*$^{CreER-}$*Bmp2*$^{fl/fl}$ mice (Fig. 6g-i). Taken together, these findings indicate that BMP2 derived from P1 stromal cells acts as a downstream effector of microbial signals, imprinting colonic iNKT cells during early-life and regulating their long-term homeostasis and response to environmental triggers.

Ortholog of P1 Stromal Cells Exist in the Early-Life Human Colon, and hrBMP2 Promotes Human iNKT Cell Proliferation

To translate our findings from mice to humans, we analyzed published fetal human

intestinal scRNA-seq data[53] to determine whether P1-like stromal cells can be identified during early human development. We focused on fibroblastic stromal cells in colon and, after quality control, analyzed 21 colon samples ranging from 8 to 22 post-conceptual weeks (PCW), and UMAP visualization identified five stromal cell clusters (Fig. 7a). To identify the human ortholog of P1 stromal cell, we examined the expression of P1 marker genes (*WNT4, ADAMDEC1, AGT,* and *FOXL1*, Fig. 1c, 4a, b) and the functional gene *BMP2* (Fig. 3d, e) across the five stromal clusters, and found that all of them were enriched in stromal cluster 1 (Fig. 7b). Additionally, feature genes specifically enriched in Day 9 mouse P1 stromal cells (C1 *Wnt4*$^{+}$ and C8 *Fgf9*$^{+}$ stromal cells, Supplementary Fig. 10a) were also highly expressed in human stromal cluster 1 (Fig. 7c). Furthermore, human stromal cluster 1 exhibited significantly higher expression of a gene module composed of the top 20 human orthologs of mouse *Wnt4*$^{+}$ stromal cell signature genes compared to other stromal clusters (Fig. 7d). These findings suggest that stromal cluster 1 in the fetal human colon transcriptionally resembles mouse P1 stromal cells. To determine the anatomical localization of cluster 1 stromal cells in the early-life human colon, we performed MERSCOPE spatial transcriptomics on both fetal (12 post-conception weeks) and neonatal (2-month-old) human colons. *EPCAM* marked epithelial cells within the mucosal layer, while *PDGFRA* labeled pan-stromal cells distributed across both the mucosal and muscularis layers (Fig. 7e; Supplementary Fig. 10b). Notably, the spatial expression of cluster 1 marker genes—including *ADAMDEC1, CXCL14,* and *BMP2* (Fig. 7b, c)—was highly enriched in the lamina propria (LP) of the mucosal layer,

with minimal expression in the muscularis (Fig. 7e; Supplementary Fig. 10b). These findings suggest that cluster 1 stromal cells are localized to the LP of the early-life human colon, resembling the anatomical positioning of mouse P1 stromal cells (Fig. 4e).

To further designate these stromal clusters based on nomenclature (S1-S4 subtypes) previously established in human fetal and adult scRNA-seq[53,54], we examined the expression of S1-S4 feature genes in all stromal cell clusters defined here (Fig. 7a). We found that fetal human colon cluster 1 stromal cells were enriched in both S1 markers (*CXCL12, FABP5, ADAMDEC1*) and S2 markers (*POSTN, F3, FRZB*) (Supplementary Fig. 10c), suggesting the P1-like stromal cells in fetal human colon is a mixture of both S1 and S2 stromal cells. Meanwhile, stromal clusters 0, 2, 3, and 4 (Fig. 7a) represented S1 (*CXCL12*), proliferating fibroblast (*MKI67, PCLAF*), S3 (*MGP, C7, DLK*), and fibroblast progenitor (*HMGA2*) clusters, respectively (Supplementary Fig. 10c)[53,54]. Interestingly, the relative cell abundance of cluster 1 stromal cells (S1+S2) was increased from 8 to 22 PCW and maintained at a higher proportion at 20-22 PCW (Supplementary Fig. 10d). This is consistent with another human gut scRNA-seq observation that the proportions of S1 and S2 are increased from 11-17 PCW, reach their peak in children, and then decrease and maintained at a lower level in adult stages[55]. These observations indicate that the cluster 1 stromal cell we identified in Fig. 7a-c is an early-life enriched population like mouse P1 cells. Together, these data support that cluster 1 stromal cell in the early-life human colon represents the human equivalent of mouse P1 stromal cell, sharing similar

transcriptomic profiles and anatomical location.

Since human P1-like stromal cells are also enriched in *BMP2* expression (Fig. 7b), we next investigated whether human iNKT cells directly respond to BMP2 *in vitro*. WINK3b.1, a high-purity clonal human $CD4^+$ iNKT cell line (Supplementary Fig. 10e) expressing BMPR1B (Fig. 7f), was cultured with human recombinant BMP2 (hrBMP2) at increasing concentrations (0, 50, 100 ng/ml) for two days. Both cell abundance and proliferation rate (Ki67 MFI) increased in an hrBMP2 dose-dependent manner, without affecting cell viability (Fig. 7g). These results demonstrate that BMP2 is sufficient to promote human iNKT cell proliferation *in vitro*. These data suggest that human P1-like stromal cell-derived BMP2 during early development plays a crucial role in iNKT cell homeostasis and may serve as a therapeutic target for preventing late-onset diseases. To test this, we pharmacologically inhibited BMP signaling in neonatal mice (Day 6 to 12 after birth) through IP injection of Dorsomorphin (Supplementary Fig. 10f). This treatment led to a significant reduction in colonic iNKT cells at Day 56 compared to vehicle-treated controls (Supplementary Fig. 10g), consistent with the early-life colonic iNKT cell suppression observed in Fig. 3k. Consequently, mice subjected to early-life BMP inhibition (Dor Oxa) exhibited protection against oxazolone-induced colitis, as evidenced by reduced weight loss (Supplementary Fig. 10h) and lower histopathological scores (Supplementary Fig. 10i) compared to control mice (Veh Oxa).

In conclusion, by integrating fetal human gut scRNA-seq and spatial transcriptomic data, we identified the human ortholog of P1 stromal cells, which highly express BMP2 and may regulate human iNKT cell homeostasis *in vivo*. These findings further underscore the clinical relevance of our mouse study in understanding early-life immune regulation and its potential implications for disease prevention.

Discussion

Early-life imprinting of mucosa-associated immune cells by the nascent microbiome is increasingly recognized to be a key determinant of health in later-life. Here, we demonstrate a critical role of a unique type of early-life associated colonic stromal cell population in regulating the long-term homeostasis and function of invariant natural killer T (iNKT) cells that play an important role in autoimmunity and host-defense against microbes. Our findings identify a previously uncharacterized *Wnt4*-expressing (so-called P1) stromal cell population that is specifically enriched in the colons of early-life mice. Further, we show that these cells produce bone morphogenetic protein 2 (BMP2), which emerges as a key factor in regulating the proliferation and accumulation of colonic iNKT cells through BMP-MAPK signaling during the critical period of life that has been coined “the window-of-opportunity” when the immune system is responsive to microbial signals associated with imprinting[10,12,21,22]. Importantly, we demonstrate that early-life microbial signals are essential for the proper regulation of P1 stromal cell abundance and BMP2 expression which impact iNKT cell homeostasis and thereby determines a fixed set-point

that persists into adulthood and influences later-life susceptibility to inflammatory and infectious diseases that are reliant on iNKT cells. Additionally, we identified a P1-like stromal cell population in the fetal human gut by analyzing single-cell RNA sequencing and spatial transcriptomic data, suggesting the potential for translating these findings from mice to human health that is actionable through manipulation of BMP2 (Supplementary Fig. 11).

As part of this work, we conducted a comprehensive classification of colonic lamina propria (LP) mesenchymal stromal cell populations in early postnatal mice under both homeostatic and embryonic macrophage-depleted conditions. We found that the composition of colonic stromal compartments differs between early and adult stages and in the presence or absence of embryonic macrophages. This notably includes a *Wnt4*$^{+}$ (P1) stromal population that is highly enriched around postnatal days 8 to 11 and gradually decreases before weaning in mice. Previous studies have suggested that early-life mesenchymal stromal cells play crucial roles in maintaining barrier tissue homeostasis by shaping intestinal epithelial cell function[25,56] and immune populations, such as dendritic cells in mesenteric lymph nodes[23] and subsets of T cells in skin[24]. Our study extends these findings by identifying a specific type of colonic *Wnt4*$^{+}$ (P1) stromal cell population that is active in determining tissue-resident iNKT cell homeostasis during early-life, but not later-life. Mechanistically, P1 stromal cells upregulate BMP2 expression compared to other stromal cells, and iNKT cells express higher levels of BMP receptors compared to

conventional αβT cells in the early-life mouse colon. RNA sequencing and *in vivo* genetic manipulation reveal that BMP2 derived from P1 stromal cells acts on BMP receptors and activates downstream non-canonical MAPK signaling in iNKT cells, thereby promoting their proliferation. This is consistent with previous findings that BMP2 can activate the MAPK pathway during osteoblast differentiation[34] and that BMPs regulate human $CD4^+$ T cell proliferation *in vitro*[57].

Precise visualization of iNKT cells in mucosal tissues, such as the intestine, is challenging due to the lack of genetic iNKT cell markers and the difficulties in applying CD1d-tetramer staining *in situ*. To overcome these challenges, we employed an adoptive transfer strategy as previously established[12] that involves the transfer of sorted $CD45.1^+$ iNKT cells into CD45.2 recipient mice during early-life. Using this approach, we not only visualized colonic iNKT cells in early postnatal mice at day 10 after birth, but also identified the components of their tissue niche that included P1 stromal cells and embryonic macrophages which were located within the crypt region of the colon LP. A previous study has shown that $CD3^+$CD1d-α-GalCer-tetramer$^+$ iNKT cells can be infrequently detected in Peyer's patches and villi of the small intestine in adult mice[58], suggesting that the localization of tissue-resident iNKT cells in the intestines is dynamic and differs between the small and large intestines during development.

Previous studies in murine models have suggested that factors such as specific types of

microbiota, chemokines that are likely derived from the intestinal epithelium and embryonic, but not bone marrow-derived, macrophages orchestrate the establishment of iNKT cell residency in the colon during a finite period within early-life[10,12,21]. These current studies highlight the previously unappreciated role of stromal cells in these processes. From this work, a broader picture of the interaction between early-life microbes and the immune system emerges in which stromal cells, whose presence and activity are determined by microbes and embryonic macrophages, are critical in defining a tissue niche within which iNKT cells reside. Under homeostatic conditions, the presence of microbes, and specifically inhibitory bacterially-derived sphingolipids[21], restrains the niche capacity by suppressing the abundance of niche components (macrophages[12] and P1 stromal cells as shown here) as well as inhibiting BMP2 expression in P1 cells. These collectively ensure a proper level of colonic iNKT cell proliferation and accumulation as resident cells during early-life. On the other hand, the absence of microbes and early-life antibiotic exposure elevates the abundance of macrophages[12] and P1 stromal cells, as well as BMP2 production, resulting in increased niche capacity, upregulated iNKT cell proliferation, and excessive colonic iNKT cell accumulation. Moreover, the increased accumulation of iNKT cells persists into adulthood and leads to hypersensitivity in experimental inflammatory bowel disease (IBD) models. Together, these studies further support the notion that susceptibility to IBD arises from microbial disruption and dysregulation of immune populations during early-life development that are consistent with clinical observations in humans associated with the hygiene (or microbe) hypothesis

and critically involves distinct types of stromal cells, as shown here[4-8].

Multiple human studies support a strong association between disruption of the BMP-MAPK signaling and IBD susceptibility. Mutations in *SMAD4* and *BMPR1A* are accompanied by chronic colonic inflammation and increased susceptibility to colitis[59,60]. In parallel, an IBD risk allele in *MAP3K8* (encoding TPL2)[61] enhances MAPK activation and pro-inflammatory cytokine production[62], while polymorphisms in *PTPN11* (encoding SHP-2), a key regulator of MAPK signaling, are associated with increased risk of ulcerative colitis[63]. Our observations call for the importance of determining actionable factors that could be applied during early-life exposures that heighten the risks of developing IBD in later-life. As such, the discovery of a novel stromal cell population that is preferentially associated with the early-life colon has led us to the identification of a human ortholog of P1 stromal cells in the fetal and neonatal colon that also exhibits enriched *BMP2* expression that we show can actively induce human iNKT cell proliferation. As iNKT cells, which produce inflammatory cytokines, are enriched in the mucosa of patients with ulcerative colitis and Crohn's disease[18,64], our studies raise the possibility that iNKT cell abundance and activity as a consequence of early-life exposures such as antibiotics can be inhibited by manipulating P1 stromal cell-derived BMP2 and thereby prevent immune dysregulation in diseases like IBD later in life.

This study raises several important questions that warrant further investigation. While we identified a close spatial association between colonic embryonic macrophages and P1 stromal cells, the mechanisms by which embryonic macrophages regulate P1 stromal cell development and function remain to be elucidated. Our single-cell RNA-seq data show that day 9 colonic macrophages express *Pdgfb* (Supplementary Data 1), suggesting a potential paracrine PDGFB-PDGFRA signaling axis that may promote the proliferation of PDGFRA$^+$ P1 stromal cells within the niche. Supporting this possibility, previous studies have demonstrated that macrophage-derived PDGFB is required for the growth of PDGFRA$^+$ fibroblasts in co-culture systems[65]. We also observed that the absence of microbiota leads to an increased abundance of P1 stromal cells and elevated *Bmp2* expression during early-life, supporting a role for microbial-derived factors in modulating the P1 niche. However, the nature of these factors and whether they indirectly influence P1 stromal cells by modulating embryonic macrophages, or act directly on *Wnt4*$^+$ stromal cells, remains unclear. Furthermore, whether early-life colonic P1 stromal cells play other roles in immune and nonimmune regulation and if similar early-life stroma-iNKT cell imprinting mechanisms operate in other barrier tissues, such as lung[10] or esophagus[66], has not been explored here but might be expected to occur. Additionally, one of the signature genes of P1 stromal cells, *Foxl1*, is known to mark subepithelial telocytes in the adult mouse intestine[67]. Whether P1 stromal cells in the early-life colon represent telocytes or their progenitors also remains an open question. Finally, although the abundance of colonic iNKT cells established during early-life is difficult to reset beyond

the “window-of-opportunity” under physiological conditions, whether there are circumstances or approaches to manipulate established iNKT cell quantities and/or activity in later-life warrants further investigation. Interestingly, multiple pharmacological approaches can modulate adult iNKT cell activity under disease conditions in adult-life; for example, glycolipid agonists such as α-galactosylceramide and cytokine interventions can enhance iNKT cell activation[14,68], whereas depleting antibodies or immunomodulatory lipid antigens can restrain excessive iNKT responses[22,69].

Methods

Mice

All the animal experiments were reviewed and approved by the Brigham and Women's Hospital Institutional Animal Care and Use Committee (OLAW Assurance A4752- 01) under Protocol #:2016N000403. Mice (C57BL/6J background) were maintained in a specific pathogen-free (SPF) barrier facility at Brigham and Women’s Hospital. Mice were housed under a controlled 12-hour light/dark cycle (lights on at 7:00 AM) at room temperature (22 ± 1^{o}C) with 60 ± 5% humidity. The following mouse strains were used: Wild type C57BL/6J (Stock No: 000664), *LysM*Cre (Stock No: 004781), *Csf1r*^{DTR} (diphtheria toxin receptor expression driven by *Csf1r* but inhibited by a loxP-flanked STOP element, Stock No: 024046), *Cx3cr1*^{GFP} (Stock No: 005582), CD45.1 (Stock No: 002014), *Pdgfra*^{CreERT2} (Stock No: 032770), and *Pdgfra*^{Cre} (Stock No: 013148) were purchased from the Jackson Laboratory. *Foxl1*$^{CreERT2\text{-}tdTomato}$ mice (Stock No: 068163) were purchased from the Mutant Mouse Resource & Research Centers (MMRRC). *Bmp2*$^{fl/fl}$ mice were generously provided by Dr. Vicki Rosen[42]. *Cd1d*$^{fl/fl}$ and *Cd1d*$^{-/-}$ mice have been previously described[49]. Germ-free (GF) C57BL/6J mice were obtained from the Massachusetts Host-Microbiome Center of the Harvard Digestive Diseases Center (Dr. Lynn Bry,

Director). MM^{DTR} mice (*LysM*Cre$^{+/-}$*Csf1r*$^{DTR+/-}$) and control littermates (*LysM*Cre$^{+/-}$ *Csf1r*$^{DTR-/-}$) were generated from the cross of *LysM*Cre$^{+/+}$ with *Csf1r*$^{DTR+/-}$ mice. *Foxl1*$^{CreER+}$*Bmp2*$^{fl/fl}$ mice and control littermates (*Foxl1*$^{CreER-}$*Bmp2*$^{fl/fl}$) were generated from the cross of *Foxl1*$^{CreERT2\text{-}tdTomato+/-}$ with *Bmp2*$^{fl/fl}$ mice. *Pdgfra*$^{CreER+}$*Bmp2*$^{fl/fl}$ mice and control littermates (*Pdgfra*$^{CreER-}$*Bmp2*$^{fl/fl}$) were generated from the cross of *Pdgfra*$^{CreERT2+/-}$ with *Bmp2*$^{fl/fl}$ mice. *Pdgfra*$^{Cre+}$*Cd1d*$^{fl/fl}$ mice and control littermates (*Pdgfra*$^{Cre-}$*Cd1d*$^{fl/fl}$) were generated from the cross of *Pdgfra*$^{Cre+/-}$ with *Cd1d*$^{fl/fl}$ mice. Age-matched male and female mice were used for all experiments.

Diphtheria toxin (DT) from *Corynebacterium* (Sigma, D0564) was dissolved in PBS (0.4 ng/μL) and administered subcutaneously at a dose of 4 ng per gram of body weight. Both experimental mice and control littermates received DT injection. Tamoxifen (TAM) (Sigma, T5648) was dissolved in corn oil (5 mg/mL) and injected intraperitoneally at 70 μg per gram of body weight. Both experimental mice and control littermates get TAM injection. Dorsomorphin (MedChem Express, HY-13418A) and vehicle (PBS/DMSO) were administered intraperitoneally at 10 μg per gram of body weight. All *in vivo* injections were performed every two days according to the schedule outlined in the manuscript.

Animals were euthanized by controlled CO_2 inhalation in accordance with institutional policies and the recommendations of the American Veterinary Medical Association (AVMA) Guidelines on Euthanasia. In all cases, a secondary method (cervical dislocation) was used to confirm euthanasia.

Human iNKT cell clone

The high-purity clonal human CD4$^+$ iNKT cell line WINK3b.1 was provided by Dr. Jenny E. Gumperz. WINK3b.1 is a clonal culture of human iNKT cells derived from a single iNKT cell isolated by flow cytometric sorting from the peripheral blood of a healthy female donor. Peripheral blood collection and research use of the sample were conducted under an approved University of Wisconsin Institutional Review Board protocol (UW IRB protocol #2018-0304), and written informed consent was obtained from the donor. WINK3b.1 were

cultured in RPMI medium supplemented with 10% heat-inactivated Fetal Bovine Serum (FBS; GeminiBio, 100-106), 5% heat-inactivated Bovine Calf Serum (Corning, 35-053-CM), 3% human AB serum (GeminiBio, 100-812), 2 mM L-glutamine (ThermoFisher, A2916801), 100 I.U./mL Penicillin and 100 µg/mL Streptomycin (ThermoFisher, 15140122), and 200 U/mL human IL-2 (Peprotech, 200-02). Cells were maintained at 37°C in a humidified incubator with 5% CO_2. For human recombinant BMP2 (hrBMP2, Gibco, PHC7145) treatment, 100,000 WINK3b.1 human iNKT cells were plated in 96-well plates. After 12 hours, cells were treated with vehicle control (acetic acid, Advanced Biomatrix, 5079), 50 ng/mL and 100 ng/mL hrBMP2 for 48 hours before harvesting for flow cytometry analysis.

Isolation of lamina propria (LP) cells

The isolation of LP cells was performed as previously described[12]. Briefly, the entire colon from postnatal and adult mice was collected, and adipose tissue was removed. The colon was opened longitudinally, washed with ice-cold PBS to remove fecal content, and cut into 2-3 cm segments. Tissue segments were placed in a 50 mL Falcon tube containing 10 mL HBSS (Gibco, 14175103) with 2mM EDTA (Fisher, BP2482-1) and shaken at 250 rpm for 45 min at 37°C. The supernatant containing epithelial cells was discarded, and the remaining LP tissue was digested in 10 mL RPMI medium (Corning, 0-040-CM) containing 10% FBS (R&D System, S11550H), 1.5% HEPES (Corning, 25-060-CI), 1 mg/mL Collagenase VIII (Sigma, C2139 [41]), and 10 µg/mL DNase I (Sigma, D5025). Digestion was performed at 250 rpm for 45 min at 37°C. Enzymatic activity was stopped by adding 10 mL ice-cold FACS buffer (PBS with 2% FBS and 1mM EDTA). The cell suspension was filtered through a 70 µm cell strainer (Fisher, 22363548), centrifuged at 500 x g for 5 min, and resuspended for flow cytometry analysis.

Isolation of thymus and spleen cells

Thymus and spleen tissues were harvested and mechanically dissociated using a 3 mL syringe plunger over a 70 µm cell strainer in a 6-well plate containing 10 mL PBS. The

cell suspension was transferred to a 50 mL Falcon tube and centrifuged at 500 x g for 5 min. Supernatants were removed, and cells were resuspended in 1 mL ACK lysing buffer (Gibco, A1049201) for 2 min to lyse red blood cells. Cells were then washed with 10 mL FACS buffer and centrifuged at 500 x g for 5 min before proceeding with flow cytometry analysis.

Flow cytometry and antibodies

Isolated tissue cells were first incubated with CD16/CD32 to block Fc receptors at 4^{o}C for 30 min, followed by staining with antibody cocktails at 4^{o}C for 30 min. SYTOX Blue stain (Invitrogen, S34857, diluted 1:1,000) was used to exclude dead cells prior to analysis. Mouse iNKT cells were identified as CD45^{+}CD3^{+}TCRβ^{+} and PBS57-loaded CD1d-tetramer positive cells. Macrophages were identified as CD45^{+}CD11b^{+}F4/80^{+} cells. Stromal cells were identified as linage (Lin: CD45, EPCAM, CD31) negative, NCAM1^{+}PDGFRA$^{+/lo}$ cells, with P1 and P2 stromal subpopulations distinguished as CD34^{-}CD9^{-} and CD34^{+}CD9^{+} cells, respectively. For cytokine stimulation to identify T cell subsets, cells were cultured in RPMI medium containing 10% FBS, 1.5% HEPES, 1X antibiotic/antimycotic (FisherScientific, 15240062), 50 ng/mL of PMA (Sigma, P1585), 0.5 μg/mL Ionomycin calcium (Sigma, 10634), and 1x Protein Transport Inhibitor (Containing Brefeldin A, BD, 555029) for 4 hours at 37 ^{o}C in 96-well plates before blocking and antibody staining. For intracellular staining, the FOXP3 transcription factor staining kit (eBioscience, 00-5523-00) was used according to the manufacturer's protocol to fix and permeabilize the cells, and LIVE/DEAD Fixable Aqua stain (Thermofisher, L34966) was used to exclude dead cells. Flow cytometry was performed using a CytoFLEX LX cytometer or a BD FACSAria II cytometer, and cell sorting was conducted on a BD FACSAria II at Harvard Medical School Flow Cytometry Core Facility. Data were analyzed using FlowJo software v10.

The following antibodies and tetramers were used for flow cytometry: PE- and APC-labeled PBS57-loaded mouse and human CD1d tetramers (NIH Tetramer Core Facility,

Atlanta, GA, diluted 1:1,000). BV785-labeled anti-mouse CD45 (clone: 30-F11, Biolegend, diluted 1:400), CD45.2 (clone: 104, Biolegend, diluted 1:400), CD4 (clone: RM4-5, Biolegend, diluted 1:400). APC-labeled anti-mouse CD3 (clone: 17A2, Biolegend, diluted 1:400), CD56/NCAM1 (clone: 809220, R&D, diluted 1:300), NK1.1 (clone: PK136, Biolegend, diluted 1:300), anti-human CD3 (clone: OKT3, Biolegend, diluted 1:400). APC/Cy7-labeled anti-mouse TCRβ (clone: H57-597, Biolegend, diluted 1:300), CD34 (clone: HM34, Biolegend, diluted 1:300), BMPR1A (Bioss, bs-1509R-APC-Cy7, diluted 1:200), IFNg (clone: xmg1.2, Biolegend, diluted 1:200), CD3, CD5 (clone:53-7.3, Biolegend, diluted 1:300), CD19 (clone: 6D5, Biolegend, diluted 1:300), Ly6G (clone: 1A8, Biolegend, diluted 1:300), NK1.1, Siglec-F (clone: E50-2440, BD, diluted 1:300), anti-human TCRα/β (clone: IP26, Biolegend, diluted 1:300). FITC-labeled anti-mouse CD11b (clone: M1/70, Biolegend, diluted 1:300), CD9 (clone: MZ3, Biolegend, diluted 1:300), Ki67 (clone: 16A8, Biolegend, diluted 1:200), CD45.1 (clone: A20, Biolegend, diluted 1:400), BMPRII (clone: E-1, Santa Cruz, diluted 1:200), GATA3 (clone: TWAJ, eBioscience, diluted 1:200), anti-human Ki67 (clone: Ki67, Biolegend, diluted 1:200). PE/Cy7 anti-mouse F4/80 (clone: BM8, Biolegend, diluted 1:300), CD45, CD31 (clone: 390, Biolegend, diluted 1:300), BMPR1B (Antibodies-online, ABIN719259, diluted 1:200), IL-17A (clone: TC11-18H10.1, Biolegend, diluted 1:200), CD19, T-bet (clone: 4B10, Biolegend, diluted 1:200), BV605-labeled anti-mouse CD140a/PDGFRA (clone: APA5, Biolegend, diluted 1:300), TCRβ, CD8 (clone: 53-6.7, Biolegend, diluted 1:400), CD45R/B220 (clone: RA3-6B2, Biolegend, diluted 1:300), CD127/IL-7Ra (clone: A7R34, Biolegend, diluted 1:300), CD11c (clone: N418, Biolegend, diluted 1:300), anti-human CD45 (clone: HI30, Biolegend, diluted 1:400), PE-labeled anti-mouse CD1d (clone: 1B1, Biolegend, diluted 1:300), RORgt (clone: B2D, eBioscience, diluted 1:200), IgA (clone: mA 6E1, eBioscience, diluted 1:300), CCR2 (clone: 475301, R&D, diluted 1:300), PE/CF594 labeled anti-mouse PLZF (clone: R17-809, BD, diluted 1:200), eFluor 450 labeled FOXP3 (clone: FJK-16s, eBioscience, diluted 1:200), EOMES (clone: Dan11mag,

eBioscience, diluted 1:200), BV421 labeled CD103 (clone: M290, BD, diluted 1:300), Alexa Fluor 700 labeled anti-mouse CD45 and I-A/I-E (clone: M5/114.15.2, Biolegend, diluted 1:300).

RNA isolation and quantitative-PCR (qPCR) assays

RNA was extracted using the RNeasy Plus Micro Kit (QIAGEN, 74134), and cDNA was synthesized using the Superscript IV VILO Master Mix (ThermoFisher, 11756500) following the manufacturer's instructions. Real-time qPCR was performed using AzuraQuant Green Fast qPCR Mix (Azura Genomics, AZ-2150) and a CFX96 Real-Time System (Bio-Rad). Gene expression levels were normalized to β-Actin (*Actb*). Primers were designed to amplify exon regions, generating products of approximately 150 bp with matched primer melting temperatures. Amplified PCR products were sequenced to confirm identity and specificity. The following primers were used: *Actb*: 5'-GATGCTCCCCGGGCTGTATT-3' and 5'-GGGGTACTTCAGGGTCAGGA-3'; *Lum*: 5'-CTCTTGCCTTGGCATTAGTCG-3' and 5'-GGGGGCAGTTACATTCTGGTG-3'; *Pdgfra:* 5'-GCAGTTGCCTTACGACTCCAGA-3' and 5'-GGTTTGAGCATCTTCACAGCCAC-3'*; Col6a1:* 5'-GACACCTCTCAGTGTGCTCTGT-3' and 5'-GCGATAAGCCTTGGCAGGAAATG-3'*; Wnt4:* 5'-AGACGTGCGAGAAACTCAAAG-3' and 5'-GGAACTGGTATTGGCACTCCT-3'; *Agt*: 5'-GCGGAGGCAAATCTGAACAA-3' and 5'-CTGCTTTGAGTTCGAGGAGGA-3'; *Adamdec1*: 5'-CCTGGGACTTCTCGGCTAC-3' and 5'-TTCGTGAGGCTTTAACTCGGG-3'; *Bmp2*: 5'-TGCACCAAGATGAACACAGC-3' and 5'-GTGCCACGATCCAGTCATTC-3' (Supplementary Table 1).

***In vitro* co-culture of primary isolated stromal cells and T cells**

FACS-sorted P1 and P2 stromal cells from early-life mice colon were plated in 96-well plates (20,000 cells/well) in RPMI medium containing 10% FBS, 1% HEPES, 1% nonessential amino acids (Gibco, 11140050), and 1X antibiotic/antimycotic for 24 hours. Adult thymic T cells (100,000 cells/well) were enriched using Pan T cell Isolation kit II

(Miltenyi Biotec, 130-095-130) and were added to the stromal cell culture wells, co-cultured for 3 days before flow cytometry analysis. For BMP signaling inhibition, 10 μM Dorsomorphin and vehicle (DMSO) were added to the stromal cell culture wells together with T cells for 3 days before flow cytometry analysis. For mouse recombinant BMP2 (mrBMP2, R&D, 5020-BP-010) treatment, 300,000 isolated thymic T cells were plated in 96 well plates and treated with vehicle (BSA/HCl, R&D, RB04), 50 ng/mL and 100 ng/mL mrBMP2 for 48 hours before analysis.

Adoptive transfer of iNKT cells

Thymic T cells were isolated from adult CD45.1 mice and stained with PE-labeled PBS57-loaded mouse CD1d tetramers (provided by the NIH tetramer core facility) at 4°C for 30 min. CD1d-tetramer-positive cells were enriched using anti-phycoerythrin (PE) MicroBeads (Miltenyi Biotec, 130-048-801) according to the manufacturer's protocol and subsequently stained with SYTOX Blue to exclude dead cells. One million sorted, live CD1d-tetramer-positive iNKT cells were then transferred via intraperitoneal injection into CD45.2 recipient mice on postnatal Day 4. Colon tissues from recipient mice were collected on postnatal Day 10 for flow cytometry and immunofluorescence (IF) staining.

Immunofluorescence and imaging

Colon tissues were harvested and fixed in 10% formalin (Fisher Scientific, 23-245-684) at room temperature (RT) for 2 hours, followed by transfer to 70% ethanol for paraffin embedding and sectioning. Paraffin dewaxing and antigen retrieval were performed as previously described[70]. Tissue sections were washed (4 × 5 min in distilled water and 1 × 5 min in PBS), blocked with 10% FBS in PBS at RT for 1 hour, and incubated with primary antibodies diluted in SignalStain Antibody Diluent (Cell Signaling Technology, 8112S) at RT for 1 hour. After washing (3 × 5 min in PBS), sections were incubated with secondary antibodies at RT for 1 hour, washed again (3 × 5 min in PBS), and counterstained with DAPI (1 μg/ml; ThermoFisher) at RT for 30 min. Slides were then rinsed in distilled water and mounted using ProLong Gold Antifade Mountant (ThermoFisher, P10144). Tissue

processing and IF staining were performed at the BIDMC Pathology Core. Fluorescence signals were captured using a Zeiss LSM 880 Confocal System, and images were analyzed using ImageJ software. The following antibodies were used for IF staining: anti-GFP (Abcam, ab6673), anti-RFP (ROCKLAND, 600-401-379), anti-mouse PDGFRA (R&D, AF1062), Alexa Fluor 647-conjugated anti-mouse CD45.1 (SouthernBiotech, 1795-31), Alexa Fluor 488-conjugated anti-goat IgG (Invitrogen, A11055) and Alexa Fluor 555-conjugated anti-rabbit IgG (Invitrogen, A31572).

Experimental oxazolone colitis model

Mice were intrarectally challenged with vehicle (50% ethanol) or 1% oxazolone in 50% ethanol (5 µl per gram of body weight) using a 3.5F catheter (Covidien, 8888160333). Body weight was monitored daily following intrarectal injection (Day 0). For histopathological analysis, colonic tissues were collected three days post-oxazolone administration (Day 3), fixed, embedded in paraffin, sectioned, and stained with hematoxylin and eosin (H&E) at the BIDMC Pathology Core. Colitis severity was assessed by pathologist Dr. Jonathan N. Glickman based on four established criteria: mononuclear inflammation, crypt hyperplasia, epithelial injury, and neutrophilic inflammation, grading on a 4-point scale (0 = absent, 1 = mild, 2 = moderate, 3 = severe), multiplied by the extent of abnormality (0:none, 1:0-10%, 2: 10-25%, 3: 25-50%, 4: >50%).

***Listeria monocytogenes* infection**

L. monocytogenes infection was performed as previously described[45]. Briefly, 8-week-old mice were inoculated via oral gavage with 3×10^9 CFUs of a mutated strain of *L. monocytogenes* with high binding affinity to mouse E-cadherin, enabling efficient infection via the oral route[71]. Colon, ileum, and mesenteric lymph nodes (mLN) were harvested 72 hours post-infection, and bacterial colony-forming units (CFUs) were enumerated.

Antibiotic treatment of animals

For antibiotic treatment experiments, breeding pairs were set up, and on the day of the offspring birth (Day 0), a cocktail of 1 g/L of ampicillin trihydrate (Goldbio, A-303-100), 1

g/L gentamicin sulfate (Goldbio, G-400-100), and 1 g/L vancomycin hydrochloride (Goldbio, V-200-25) was added to the drinking water of the breeding pairs. Water was replaced weekly, and offspring were switched to normal drinking water after weaning (Day 21).

Bulk RNA sequencing

Total RNA from whole colon tissue of CT and MM^{DTR} mice was extracted using the RNeasy Plus Mini Kit (QIAGEN, 74134) and used as input material. Library preparation and transcriptome sequencing were performed by Novogene Bioinformatics Technology Co., Ltd. using an Illumina HiSeq X Ten platform to generate 150-bp paired-end reads. For bulk RNA sequencing of FACS-sorted cells, enzyme-digested colon lamina propria (LP) cells were washed once with 1% BSA/PBS and resuspended in 1% BSA/PBS for sorting. Two hundred P1 ($Lin^-NCAM1^+PDGFRA^{lo}CD34^-CD9^-$) or P2 ($Lin^-NCAM1^+PDGFRA^+CD34^+CD9^+$) stromal cells from Day 9 or Day 15 wild-type (WT) mice, 200 conventional αβT cells and 50 iNKT cells from Day 9 WT mice, as well as 50 iNKT cells from Day 9 CT and MM^{DTR} mice, were sorted using a BD FACSAria II into lysis buffer (0.2% Triton X-100 solution with RNase inhibitor) and used as input material. Double strand cDNA was generated following the SMART-seq2 protocol as previously described[72]. Briefly, homogenized cells in lysis buffer were added with Oligo-dT and dNTP and incubated at 72°C for 3 min. First-strand cDNA was synthesized using SuperScript II reverse transcriptase (Invitrogen, 18064014) and template switch oligo (TSO) primer, followed by PCR amplification using KAPA HiFi HotStart ReadyMix (Roche, 7958935001) and an ISPCR primer. Amplified cDNA libraries were purified with AMPure XP beads (Beckman Coulter, A63881). Library preparation (Illumina Nextera XT) and sequencing were performed at the Biopolymers Facility at Harvard Medical School using an Illumina NextSeq 500 sequencer to generate 75-bp paired-end reads.

FASTQ raw data were uploaded to Partek Flow (Partek, building version: 10.0.21.0201) and analyzed with the default setting. Briefly, trimmed reads were aligned to the mouse

genome (GRCm38/mm10) using STAR 2.5.3a, and gene expression was quantified using the Partek E/M annotation model with a default setting. Downstream analyses were conducted in RStudio (2024.09.1+394). Low-expressed genes (counts=0 in more than 50% of the samples) were filtered out before analysis. Differentially expressed genes (DEGs) were identified using the DESeq2 (1.46.0) package, with significance defined as an adjusted *P*-value < 0.05 and a $\log_2$ |fold-change| > 1. DEGs lists were analyzed for pathway enrichment using the Metascape website (http://metascape.org/gp/index.html#/main/step1)[73]. Principal component analysis (PCA) and volcano plots were generated using ggplot2 (3.5.1) package, and heatmaps of selected genes were generated using pheatmap (1.0.12) package with $\log_2$(TPM+1) transformed data.

Single-cell RNA-sequencing

Whole colon LP cells were isolated from three CT and three MM^{DTR} mice and pooled by group. Live cells were FACS-sorted for single-cell RNA sequencing, which was performed by the Brigham and Women's Hospital Single Cell Genomics Core. Briefly, sorted live cells were separated into a single droplet using the Chromium Single Cell 3' v3 kit (10X Genomics) according to the manufacturer's protocol. The libraries were then sequenced on the NovaSeq 6000 S2 platform. Raw data reads were aligned to the mouse transcriptome (mm10) using the Cell Ranger toolkit (version 3.0.1), which was also used for cell selection, filtering, and unique molecular identifier (UMI) counting. Single-cell RNA-seq data of adult colon LP cells were downloaded from the NCBI GEO database (GSE172261), and healthy control mice data were filtered for analysis.

Data analysis was performed using the Seurat (5.1.0)[74] package in RStudio. For quality control, cells with counts of 200 to 5,000 genes and less than 5% mitochondrial genes were kept. A total of 4,982 cells from Day 9 CT mice and 4,672 cells from MM^{DTR} mice were analyzed. Normalization, variable gene selection, data integration, and scaling were performed using standard Seurat settings. Uniform Manifold Approximation and

Projection (UMAP) was performed using 20 principal components (PCs), and clustering was conducted with a resolution parameter of 0.5, identifying 16 clusters. Feature genes and differentially expressed genes between CT and MM^{DTR} clusters were identified using the Seurat "FindMarkers" function. For Day 9 vs. adult mouse comparisons, adult mice data were down-sampled to 6,000 cells (200 to 5,000 genes per cell, < 5% mitochondrial genes) for analysis. A total of 15 clusters were identified using a resolution parameter of 0.3. The cell identities of each cluster were annotated based on known colon LP cell marker genes. For human fetal colon scRNA-seq analysis, processed "fibroblast" data were downloaded from the STAR-FINDer Single Cell and Spatial Transcriptomics Data Portal[53] (https://simmonslab.shinyapps.io/FetalAtlasDataPortal). Colon cells with counts of 200 to 5,000 genes and less than 5% mitochondrial gene content were retained, resulting in a total of 15,540 cells from 21 human samples for downstream analysis. Clustering was performed using a resolution parameter of 0.1, identifying six distinct clusters. Erythroid cells were excluded, and the remaining five stromal cell clusters were used for downstream feature gene expression analysis.

Human sample collection, handling and processing

Samples were collected during clinically indicated procedures, in accordance with local and national patient safety guidelines, with informed consent, and under approval from the North of Scotland Research Ethics Committee 2 (MIMIC Study, Ethics Reference: 22/NS/0027). Pediatric samples were obtained from children undergoing intestinal resection for various intestinal pathologies, with tissue sampled from unaffected resection margins that were surplus to histopathological requirements. The operating surgeon collected surgical specimens and immediately placed on ice in Dulbecco's Modified Eagle Medium (DMEM) supplemented with 10% fetal calf serum (FCS; Sigma-Aldrich), 100 U/mL penicillin, and 100 µg/mL streptomycin (Sigma-Aldrich), then processed without delay. Fetal intestinal tissues were initially collected and processed by the Human Developmental Biology Resource (HDBR), London. Following appropriate consent and

approval from the London – Fulham Research Ethics Committee (HDBR Project 200659, REC: 18/LO/0822), intestinal tissue was dissected and placed in Leibovitz's L-15 medium (Sigma) on ice before transfer to Oxford. Upon arrival, pediatric and fetal tissues were washed in phosphate-buffered saline (PBS) and either immediately cryopreserved in CryoStor CS10 medium (Sigma-Aldrich) to minimize batch effects or fixed in formalin, as described previously[53]. For formalin-fixed, paraffin-embedded (FFPE) processing, tissues were fixed in formalin for 48 hours, transferred to 70% ethanol, and embedded in paraffin wax through a standard graded series.

MERSCOPE

High-resolution subcellular spatial transcriptomics was performed using the Vizgen MERSCOPE platform according to the manufacturer's guidelines for resistant tissues (Vizgen, MERSCOPE, 91600112, Rev B), with minor modifications. FFPE sections from pediatric and fetal samples were cut at 5 µm thickness and mounted onto MERSCOPE-compatible slides. Slides were incubated at 55^{o}C for 15 minutes and air-dried for 2 hours before storage at -20^{o}C for a maximum of 3 days. Sections then underwent deparaffinization, cell boundary staining, anchoring, gel embedding, a 6-hour digestion step, and extended clearing. Autofluorescence quenching was performed for 6 hours prior to probe hybridization. Custom probes were hybridized to the tissue for 68 hours before imaging on the MERSCOPE platform (Vizgen, 91600001, Rev F).

Spatial transcriptomics data analysis

Raw MERSCOPE image data were processed and transcripts decoded using onboard MERlin (v0.1.6) software with a custom gene panel codebook. The target gene panel was curated by in-house intestinal biology experts, referencing published fetal and pediatric scRNA-seq datasets. In situ spatial transcriptomics data from MERSCOPE platform was re-segmented using Baysor algorithm[75], version 0.7.0. Transcripts associated with negative control codewords or blanks were removed. Remaining transcripts were segmented into cells using Baysor with Cellpose-derived cell boundary priors.

Segmentation prior confidence was set to 0.7. Prior segmentation data also informed estimates of average cell size. The number of expected clusters (n-clusters) was determined via Louvain clustering at a resolution of 0.7. Cell-by-gene count matrices were generated from re-segmented transcript assignments. Transcripts with a posterior probability < 0.9 or those not confidently assigned to a single cell (< 0.9) were excluded. Resulting matrices, along with cell boundary coordinates, were imported into Seurat (version 5.1.0) in R for quality control (QC), clustering, and visualization. QC filtering excluded cells with fewer than 15 detected transcripts or >10% negative control transcripts. Very small cells (<1st percentile of size distribution) lacking nuclei were presumed to be fragments and removed. Similarly, oversized cells (>99th percentile) were excluded as likely segmentation artifacts. Cells outside tissue regions were filtered out if they had fewer than five neighboring cells. Additional cells in regions of tissue folds, detachment, or poor morphology were manually removed. Gene expression data were normalized using Seurat's SCTransform(). For large slides, Seurat's sketch workflow was applied. Datasets were split into samples, and 2,500 cells per sample were selected using SketchData(). Data were scaled with ScaleData() and dimensionality reduced using RunPCA(). Integration was performed using IntegrateLayers() with the RPCA method. Cells were clustered using FindClusters() and visualized with RunUMAP(). The full dataset was projected using ProjectIntegration() and ProjectData() to generate final results.

Statistical analysis

Statistical analyses were performed using GraphPad Prism v10. Statistical significance was determined as described in the figure legends. An unpaired Student's t-test was used for comparisons between two groups. One-way ANOVA followed by Dunnett's multiple comparisons test was used for comparisons among multiple groups. Two-way ANOVA followed by Sidak's or Tukey's multiple comparisons tests was used for multiple groups with multiple conditions. Differences were considered statistically significant at $P < 0.05$.

Data availability

The raw files for the bulk RNA-seq and single-cell RNA-seq data generated in the current study have been deposited in the GEO database under the GSE297816 (https://www.ncbi.nlm.nih.gov/geo/query/acc.cgi?acc=GSE297816). The MERSCOPE data have been deposited in Zenodo under the 10.5281/zenodo.19450420 (https://doi.org/10.5281/zenodo.19450420). Previously published single-cell RNA-seq data of adult mice colon LP cells are available through GEO database under the GSE172261 (https://www.ncbi.nlm.nih.gov/geo/query/acc.cgi?acc=GSE172261)[32], human colon single-cell RNA-seq data are available through GEO database under the GSE158702 (https://www.ncbi.nlm.nih.gov/geo/query/acc.cgi?acc=GSE158702)[53]. The raw numbers for graphs are available in the Source Data file whenever possible. The source data are provided with this paper.

Code availability

All data were analyzed using established, published pipelines with parameters detailed in the "Methods" section. Analysis scripts for bulk RNA-seq data, single-cell RNA-seq data are available from GitHub (https://github.com/xilin93/early-life-colon-stromal-cell-regulate-iNKT-cells), and for MERSCOPE data are available from GitHub (https://github.com/antanaviciutegroup/wnt4-fib-merscope).

References

1 Belkaid, Y. & Hand, T. W. Role of the microbiota in immunity and inflammation. *Cell* **157**, 121-141 (2014). https://doi.org/10.1016/j.cell.2014.03.011

2 Gensollen, T., Iyer, S. S., Kasper, D. L. & Blumberg, R. S. How colonization by microbiota in early life shapes the immune system. *Science* **352**, 539-544 (2016). https://doi.org/10.1126/science.aad9378

3 Al Nabhani, Z. & Eberl, G. Imprinting of the immune system by the microbiota early in life. *Mucosal Immunol* **13**, 183-189 (2020). https://doi.org/10.1038/s41385-020-0257-y

4 Strachan, D. P. Hay fever, hygiene, and household size. *BMJ* **299**, 1259-1260 (1989). https://doi.org/10.1136/bmj.299.6710.1259

5 Shaw, S. Y., Blanchard, J. F. & Bernstein, C. N. Association between the use of

antibiotics in the first year of life and pediatric inflammatory bowel disease. *Am J Gastroenterol* **105**, 2687-2692 (2010). https://doi.org/10.1038/ajg.2010.398

6 Hviid, A., Svanstrom, H. & Frisch, M. Antibiotic use and inflammatory bowel diseases in childhood. *Gut* **60**, 49-54 (2011). https://doi.org/10.1136/gut.2010.219683

7 Kamphorst, K. *et al.* Early life antibiotics and childhood gastrointestinal disorders: a systematic review. *BMJ Paediatr Open* **5**, e001028 (2021). https://doi.org/10.1136/bmjpo-2021-001028

8 Agrawal, M. *et al.* Early-Life Mebendazole Exposure Increases the Risk of Adult-Onset Ulcerative Colitis: A Population-Based Cohort Study. *Am J Gastroenterol* **117**, 2025-2032 (2022). https://doi.org/10.14309/ajg.0000000000001933

9 Constantinides, M. G. & Belkaid, Y. Early-life imprinting of unconventional T cells and tissue homeostasis. *Science* **374**, eabf0095 (2021). https://doi.org/10.1126/science.abf0095

10 Olszak, T. *et al.* Microbial exposure during early life has persistent effects on natural killer T cell function. *Science* **336**, 489-493 (2012). https://doi.org/10.1126/science.1219328

11 Bendelac, A. Positive selection of mouse NK1+ T cells by CD1-expressing cortical thymocytes. *J Exp Med* **182**, 2091-2096 (1995). https://doi.org/10.1084/jem.182.6.2091

12 Gensollen, T. *et al.* Embryonic macrophages function during early life to determine invariant natural killer T cell levels at barrier surfaces. *Nat Immunol* **22**, 699-710 (2021). https://doi.org/10.1038/s41590-021-00934-0

13 Cui, G., Abe, S., Kato, R. & Ikuta, K. Insights into the heterogeneity of iNKT cells: tissue-resident and circulating subsets shaped by local microenvironmental cues. *Front Immunol* **15**, 1349184 (2024). https://doi.org/10.3389/fimmu.2024.1349184

14 Kawano, T. *et al.* CD1d-restricted and TCR-mediated activation of valpha14 NKT cells by glycosylceramides. *Science* **278**, 1626-1629 (1997). https://doi.org/10.1126/science.278.5343.1626

15 Benlagha, K., Weiss, A., Beavis, A., Teyton, L. & Bendelac, A. In vivo identification of glycolipid antigen-specific T cells using fluorescent CD1d tetramers. *J Exp Med* **191**, 1895-1903 (2000). https://doi.org/10.1084/jem.191.11.1895

16 Matsuda, J. L. *et al.* Tracking the response of natural killer T cells to a glycolipid antigen using CD1d tetramers. *J Exp Med* **192**, 741-754 (2000). https://doi.org/10.1084/jem.192.5.741

17 Crosby, C. M. & Kronenberg, M. Tissue-specific functions of invariant natural killer T cells. *Nat Rev Immunol* **18**, 559-574 (2018). https://doi.org/10.1038/s41577-018-0034-2

18 Burrello, C. *et al.* Mucosa-associated microbiota drives pathogenic functions in IBD-derived intestinal iNKT cells. *Life Sci Alliance* **2** (2019). https://doi.org/10.26508/lsa.201800229

19 Iyer, S. S. *et al.* Dietary and Microbial Oxazoles Induce Intestinal Inflammation by Modulating Aryl Hydrocarbon Receptor Responses. *Cell* **173**, 1123-1134 e1111 (2018). https://doi.org/10.1016/j.cell.2018.04.037

20 Heller, F., Fuss, I. J., Nieuwenhuis, E. E., Blumberg, R. S. & Strober, W. Oxazolone colitis, a Th2 colitis model resembling ulcerative colitis, is mediated by IL-13-producing NK-T cells. *Immunity* **17**, 629-638 (2002). https://doi.org/10.1016/s1074-7613(02)00453-3

21 An, D. *et al.* Sphingolipids from a symbiotic microbe regulate homeostasis of host intestinal natural killer T cells. *Cell* **156**, 123-133 (2014). https://doi.org/10.1016/j.cell.2013.11.042

22 Oh, S. F. *et al.* Host immunomodulatory lipids created by symbionts from dietary amino acids. *Nature* **600**, 302-307 (2021). https://doi.org/10.1038/s41586-021-04083-0

23 Pezoldt, J. *et al.* Neonatally imprinted stromal cell subsets induce tolerogenic dendritic cells in mesenteric lymph nodes. *Nat Commun* **9**, 3903 (2018). https://doi.org/10.1038/s41467-018-06423-7

24 Boothby, I. C. *et al.* Early-life inflammation primes a T helper 2 cell-fibroblast niche in skin. *Nature* **599**, 667-672 (2021). https://doi.org/10.1038/s41586-021-04044-7

25 Jacob, J. M. *et al.* PDGFRalpha-induced stromal maturation is required to restrain postnatal intestinal epithelial stemness and promote defense mechanisms. *Cell Stem Cell* **29**, 856-868 e855 (2022). https://doi.org/10.1016/j.stem.2022.04.005

26 McCarthy, N., Kraiczy, J. & Shivdasani, R. A. Cellular and molecular architecture of the intestinal stem cell niche. *Nat Cell Biol* **22**, 1033-1041 (2020). https://doi.org/10.1038/s41556-020-0567-z

27 Degirmenci, B., Valenta, T., Dimitrieva, S., Hausmann, G. & Basler, K. GLI1-expressing mesenchymal cells form the essential Wnt-secreting niche for colon stem cells. *Nature* **558**, 449-453 (2018). https://doi.org/10.1038/s41586-018-0190-3

28 McCarthy, N. *et al.* Distinct Mesenchymal Cell Populations Generate the Essential Intestinal BMP Signaling Gradient. *Cell Stem Cell* **26**, 391-402 e395 (2020). https://doi.org/10.1016/j.stem.2020.01.008

29 Barnhoorn, M. C. *et al.* Stromal Cells in the Pathogenesis of Inflammatory Bowel Disease. *J Crohns Colitis* **14**, 995-1009 (2020). https://doi.org/10.1093/ecco-jcc/jjaa009

30 Strong, S. A., Pizarro, T. T., Klein, J. S., Cominelli, F. & Fiocchi, C. Proinflammatory cytokines differentially modulate their own expression in human intestinal mucosal mesenchymal cells. *Gastroenterology* **114**, 1244-1256 (1998). https://doi.org/10.1016/s0016-5085(98)70431-7

31 Nowarski, R., Jackson, R. & Flavell, R. A. The Stromal Intervention: Regulation of Immunity and Inflammation at the Epithelial-Mesenchymal Barrier. *Cell* **168**, 362-375 (2017). https://doi.org/10.1016/j.cell.2016.11.040

32 Jasso, G. J. *et al.* Colon stroma mediates an inflammation-driven fibroblastic response controlling matrix remodeling and healing. *PLoS Biol* **20**, e3001532 (2022). https://doi.org/10.1371/journal.pbio.3001532

33 Zhang, W. & Liu, H. T. MAPK signal pathways in the regulation of cell proliferation in mammalian cells. *Cell Res* **12**, 9-18 (2002). https://doi.org/10.1038/sj.cr.7290105

34 Huang, R. L., Yuan, Y., Tu, J., Zou, G. M. & Li, Q. Opposing TNF-alpha/IL-1beta- and BMP-2-activated MAPK signaling pathways converge on Runx2 to regulate BMP-2-induced osteoblastic differentiation. *Cell Death Dis* **5**, e1187 (2014). https://doi.org/10.1038/cddis.2014.101

35 Wang, R. N. *et al.* Bone Morphogenetic Protein (BMP) signaling in development and human diseases. *Genes Dis* **1**, 87-105 (2014). https://doi.org/10.1016/j.gendis.2014.07.005

36 Zhang, Y. & Que, J. BMP Signaling in Development, Stem Cells, and Diseases of the Gastrointestinal Tract. *Annu Rev Physiol* **82**, 251-273 (2020). https://doi.org/10.1146/annurev-physiol-021119-034500

37 Cargnello, M. & Roux, P. P. Activation and function of the MAPKs and their substrates, the MAPK-activated protein kinases. *Microbiol Mol Biol Rev* **75**, 50-83 (2011). https://doi.org/10.1128/MMBR.00031-10

38 Sanchez-Duffhues, G., Williams, E., Goumans, M. J., Heldin, C. H. & Ten Dijke, P. Bone morphogenetic protein receptors: Structure, function and targeting by selective small molecule kinase inhibitors. *Bone* **138**, 115472 (2020). https://doi.org/10.1016/j.bone.2020.115472

39 Kobayashi, A. *et al.* Six2 defines and regulates a multipotent self-renewing nephron progenitor population throughout mammalian kidney development. *Cell Stem Cell* **3**, 169-181 (2008). https://doi.org/10.1016/j.stem.2008.05.020

40 Kolev, H. M. *et al.* A FoxL1-CreERT-2A-tdTomato Mouse Labels Subepithelial Telocytes. *Cell Mol Gastroenterol Hepatol* **12**, 1155-1158 e1154 (2021). https://doi.org/10.1016/j.jcmgh.2021.05.009

41 Jung, S. *et al.* Analysis of fractalkine receptor CX(3)CR1 function by targeted deletion and green fluorescent protein reporter gene insertion. *Mol Cell Biol* **20**, 4106-4114 (2000). https://doi.org/10.1128/MCB.20.11.4106-4114.2000

42 Bandyopadhyay, A. *et al.* Genetic analysis of the roles of BMP2, BMP4, and BMP7 in limb patterning and skeletogenesis. *PLoS Genet* **2**, e216 (2006). https://doi.org/10.1371/journal.pgen.0020216

43 Kang, S. H., Fukaya, M., Yang, J. K., Rothstein, J. D. & Bergles, D. E. NG2+ CNS glial progenitors remain committed to the oligodendrocyte lineage in postnatal life and following neurodegeneration. *Neuron* **68**, 668-681 (2010). https://doi.org/10.1016/j.neuron.2010.09.009

44 Arrunategui-Correa, V. & Kim, H. S. The role of CD1d in the immune response against Listeria infection. *Cell Immunol* **227**, 109-120 (2004).

https://doi.org/10.1016/j.cellimm.2004.02.003

45 Zhang, T. *et al.* Deciphering the landscape of host barriers to Listeria monocytogenes infection. *Proc Natl Acad Sci U S A* **114**, 6334-6339 (2017). https://doi.org/10.1073/pnas.1702077114

46 Matsuda, J. L. *et al.* Homeostasis of V alpha 14i NKT cells. *Nat Immunol* **3**, 966-974 (2002). https://doi.org/10.1038/ni837

47 McNab, F. W. *et al.* The influence of CD1d in postselection NKT cell maturation and homeostasis. *J Immunol* **175**, 3762-3768 (2005). https://doi.org/10.4049/jimmunol.175.6.3762

48 Wei, D. G. *et al.* Expansion and long-range differentiation of the NKT cell lineage in mice expressing CD1d exclusively on cortical thymocytes. *J Exp Med* **202**, 239-248 (2005). https://doi.org/10.1084/jem.20050413

49 Olszak, T. *et al.* Protective mucosal immunity mediated by epithelial CD1d and IL-10. *Nature* **509**, 497-502 (2014). https://doi.org/10.1038/nature13150

50 Kayama, H., Okumura, R. & Takeda, K. Interaction Between the Microbiota, Epithelia, and Immune Cells in the Intestine. *Annu Rev Immunol* **38**, 23-48 (2020). https://doi.org/10.1146/annurev-immunol-070119-115104

51 Zheng, D., Liwinski, T. & Elinav, E. Interaction between microbiota and immunity in health and disease. *Cell Res* **30**, 492-506 (2020). https://doi.org/10.1038/s41422-020-0332-7

52 Constantinides, M. G. & Bendelac, A. Transcriptional regulation of the NKT cell lineage. *Curr Opin Immunol* **25**, 161-167 (2013). https://doi.org/10.1016/j.coi.2013.01.003

53 Fawkner-Corbett, D. *et al.* Spatiotemporal analysis of human intestinal development at single-cell resolution. *Cell* **184**, 810-826 e823 (2021). https://doi.org/10.1016/j.cell.2020.12.016

54 Kinchen, J. *et al.* Structural Remodeling of the Human Colonic Mesenchyme in Inflammatory Bowel Disease. *Cell* **175**, 372-386 e317 (2018). https://doi.org/10.1016/j.cell.2018.08.067

55 Elmentaite, R. *et al.* Cells of the human intestinal tract mapped across space and time. *Nature* **597**, 250-255 (2021). https://doi.org/10.1038/s41586-021-03852-1

56 Kim, J. E. *et al.* Gut microbiota promotes stem cell differentiation through macrophage and mesenchymal niches in early postnatal development. *Immunity* **55**, 2300-2317 e2306 (2022). https://doi.org/10.1016/j.immuni.2022.11.003

57 Martinez, V. G. *et al.* The BMP Pathway Participates in Human Naive CD4+ T Cell Activation and Homeostasis. *PLoS One* **10**, e0131453 (2015). https://doi.org/10.1371/journal.pone.0131453

58 Johnson, D. N. *et al.* Differential location of NKT and MAIT cells within lymphoid tissue. *Sci Rep* **12**, 4034 (2022). https://doi.org/10.1038/s41598-022-07704-4

59 Szigeti, R. *et al.* SMAD4 haploinsufficiency associates with augmented colonic inflammation in select humans and mice. *Ann Clin Lab Sci* **42**, 401-408 (2012).

60 MacFarland, S. P. *et al.* Gastrointestinal Polyposis in Pediatric Patients. *J Pediatr Gastroenterol Nutr* **69**, 273-280 (2019). https://doi.org/10.1097/MPG.0000000000002421

61 Jostins, L. *et al.* Host-microbe interactions have shaped the genetic architecture of inflammatory bowel disease. *Nature* **491**, 119-124 (2012). https://doi.org/10.1038/nature11582

62 Hedl, M. & Abraham, C. A TPL2 (MAP3K8) disease-risk polymorphism increases TPL2 expression thereby leading to increased pattern recognition receptor-initiated caspase-1 and caspase-8 activation, signalling and cytokine secretion. *Gut* **65**, 1799-1811 (2016). https://doi.org/10.1136/gutjnl-2014-308922

63 Narumi, Y. *et al.* Polymorphisms of PTPN11 coding SHP-2 as biomarkers for ulcerative colitis susceptibility in the Japanese population. *J Clin Immunol* **29**, 303-310 (2009). https://doi.org/10.1007/s10875-008-9272-6

64 Fuss, I. J. *et al.* Nonclassical CD1d-restricted NK T cells that produce IL-13 characterize an atypical Th2 response in ulcerative colitis. *J Clin Invest* **113**, 1490-1497 (2004). https://doi.org/10.1172/JCI19836

65 Zhou, X. *et al.* Circuit Design Features of a Stable Two-Cell System. *Cell* **172**, 744-757 e717 (2018). https://doi.org/10.1016/j.cell.2018.01.015

66 Lexmond, W. S. *et al.* Involvement of the iNKT cell pathway is associated with early-onset eosinophilic esophagitis and response to allergen avoidance therapy. *Am J Gastroenterol* **109**, 646-657 (2014). https://doi.org/10.1038/ajg.2014.12

67 Shoshkes-Carmel, M. *et al.* Subepithelial telocytes are an important source of Wnts that supports intestinal crypts. *Nature* **557**, 242-246 (2018). https://doi.org/10.1038/s41586-018-0084-4

68 Bharadwaj, N. S. & Gumperz, J. E. Harnessing invariant natural killer T cells to control pathological inflammation. *Front Immunol* **13**, 998378 (2022). https://doi.org/10.3389/fimmu.2022.998378

69 Scheuplein, F. *et al.* A humanized monoclonal antibody specific for invariant Natural Killer T (iNKT) cells for in vivo depletion. *PLoS One* **8**, e76692 (2013). https://doi.org/10.1371/journal.pone.0076692

70 Zaqout, S., Becker, L. L. & Kaindl, A. M. Immunofluorescence Staining of Paraffin Sections Step by Step. *Front Neuroanat* **14**, 582218 (2020). https://doi.org/10.3389/fnana.2020.582218

71 Wollert, T. *et al.* Extending the host range of Listeria monocytogenes by rational protein design. *Cell* **129**, 891-902 (2007). https://doi.org/10.1016/j.cell.2007.03.049

72 Picelli, S. *et al.* Full-length RNA-seq from single cells using Smart-seq2. *Nat Protoc* **9**, 171-181 (2014). https://doi.org/10.1038/nprot.2014.006

73 Zhou, Y. *et al.* Metascape provides a biologist-oriented resource for the analysis of systems-level datasets. *Nat Commun* **10**, 1523 (2019). https://doi.org/10.1038/s41467-019-09234-6

74 Stuart, T. *et al.* Comprehensive Integration of Single-Cell Data. *Cell* **177**, 1888-1902 e1821 (2019). https://doi.org/10.1016/j.cell.2019.05.031

75 Petukhov, V. *et al.* Cell segmentation in imaging-based spatial transcriptomics. *Nat Biotechnol* **40**, 345-354 (2022). https://doi.org/10.1038/s41587-021-01044-w

Acknowledgments

We thank the Blumberg laboratory members for their assistance with manuscript preparation, and especially Yuly Lopera for assistance with animal husbandry. We thank Dr. Dale I. Godfrey for valuable input and discussion on the manuscript. We thank Brigham and Women's Hospital Single Cell Genomics Core for performing scRNA-seq, Harvard Medical School Flow Cytometry Core Facility for helping with the FACS experiments, Dr. Susan Hagen and the BIDMC Pathology Core Facility for performing the IF staining, Dr. Lynn Bry and the Massachusetts host-microbiome center for providing Germ-Free mice.

Funding

RSB discloses support for the research and publication of this work from the NIH grants (DK044319, DK051362, DK088199, and 5P01AI073748) and the Harvard Digestive Diseases Center (P30DK034854). XL discloses support for the research and publication of this work from the Crohn's and Colitis Foundation of America Research Fellow Award (1282671). AA, CHL, and AS disclose support for the research of this work from the Chan Zuckerberg Initiative Foundation (DAF2021-237606). TG discloses support for the research of this work from the Fondation pour la Recherche Médicale (AJE202210016199) and the Association pour la Recherche contre le Cancer (ARCPJA2024080008675). TZ, TH, JNG, NSB, VR, JEG, and MKW declare no relevant funding.

Author contributions

XL, TG, and RSB conceived, designed, and interpreted the experiments. AA, CHL, and AS performed MERSCOPE of human colon samples and interpreted the data. XL, TZ, TH, MKW, and JNG carried out the experiments and interpreted the data. NSB and JEG provided the human iNKT cell line WINK3b.1. VR provided *Bmp2*$^{fl/fl}$ mice. XL and RSB wrote the manuscript. All authors were involved in the critical revision of the manuscript for important intellectual content.

Competing interests

The Authors declare no competing interests.

Figure Legends

Fig. 1 | A *Wnt4*$^{+}$ stromal cell population is significantly reduced following early-life macrophage depletion. (a-d) Single-cell RNA sequencing (scRNA-seq) of Day 9 live cells sorted from the colon lamina propria of control (CT) *LysCre*$^{+/-}$*Csf1r*$^{DTR-/-}$ mice (n = 3 mice, 4,982 cells) and macrophage-depleted (MM^{DTR}) *LysCre*$^{+/-}$*Csf1r*$^{DTR+/-}$ mice (n = 3 mice, 4,672 cells) after diphtheria toxin (DT) administration from Day 6 to 8 after birth. **(a)** Unsupervised UMAP clustering of scRNA-seq data. **(b)** Changes in relative cluster abundance of MM^{DTR} compared to CT mice are shown as the percentage of each cluster relative to the total cell count. The red arrow indicates C1 *Wnt4*$^{+}$ stromal cells. **(c)** Violin plot showing the expression of *Wnt4, Agt*, and *Adamdec1*. **(d)** Feature plots displaying *Wnt4*, *Pdgfra, Ncam1, Cd34*, and *Cd9* expression. Red circles indicate C1 *Wnt4*$^{+}$ stromal cells and C8 *Fgf9*$^{+}$ stromal cells (P1), while the blue circle marks other stromal cells (P2). **(e)** Flow cytometry gating strategy for identifying P1 and P2 stromal cell populations. **(f)** Quantitative PCR (qPCR) analysis of *Wnt4, Agt*, and *Adamdec1* in sorted Day 9 P1 (n=3) and P2 (n=3) stromal cells. **(g, h)** Representative flow cytometry plots (left) and quantification of colonic macrophages and iNKT cells **(g)**, as well as P1 and P2 stromal cells **(h)** in CT (n=5) and MM^{DTR} (n=7) mice at Day 9 after DT administration. Data are presented as mean ± SD. *P* values were calculated by unpaired two-sided Student's t-test **(f-h)**. $P < 0.05$ is considered statistically significant. Each symbol **(f-h)** represents one individual mouse. Data **(f-h)** are representative of three independent experiments. Source data are provided as a Source Data file.

Fig. 2 | P1 (*Wnt4*$^{+}$) stromal cells are highly enriched before Day 10 of postnatal life and support thymic iNKT cell proliferation in co-culture. (a) Images of primary isolated P1 and P2 stromal cells from Day 9 mouse colons cultured for 24 and 96 hours. Scale bar, 50 µm. **(b-d)** Representative flow cytometry plots (left), absolute numbers of CD1d tetramer-positive thymic iNKT cells **(b)**, Ki67 mean fluorescence intensity (MFI) of iNKT cells **(c)**, and total thymic T cell survival rates **(d)** in cultures with P1 (n=6), P2 (n=6), or without stromal cells (n=6) at 3 days post-culture. **(e, f)** Representative flow cytometry plots (left), Ki67 MFI of colonic and splenic iNKT cells (n=4 per group) **(e)**, and proportions of P1 (red) and P2 (blue) stromal cells among total stromal cells (D5 n=4, D8 n=4, D9 n=5, D10 n=4, D11 n=4, D15 n=8, D18 n=4, D20 n=4) **(f)** in WT mice at early postnatal stages. **(g-i)** scRNA-seq analysis of colon LP cells from Day 9 CT (4,982 cells) and adult WT (6,000 cells) mice. **(g)** Unsupervised UMAP clustering. **(h)** Feature plots of *Wnt4* and *Agt* expression, with red circles marking *Wnt4*$^{+}$ stromal cells and gray circles indicating all stromal clusters. **(i)** Proportions of *Wnt4*$^{+}$ stromal cells within all stromal cells in Day 9 CT and adult WT mice. **(j, k)** Representative flow cytometry plots (left), absolute numbers of thymic iNKT cells **(j)**, and Ki67 MFI of iNKT cells **(k)** 3 days post-co-culture with primary P1 stromal cells isolated from WT mice colons at Day 9 and Day 15 (n=8 per group). Data are presented as mean ± SD. P values were calculated by one-way ANOVA with Dunnett's

multiple comparisons test **(b-d)**, two-way ANOVA with Sidak's multiple comparisons test **(e)**, and unpaired two-sided Student's t-test **(j, k)**. $P < 0.05$ is considered statistically significant. Each symbol **(b-e, j, k)** represents one individual mouse. Data **(b-e, j, k)** are representative of three independent experiments. Source data are provided as a Source Data file.

Fig. 3 | Early-life P1 (*Wnt4*$^+$) stromal cells promote colonic iNKT cell proliferation via BMP-MAPK signaling. (a-d) Bulk RNA-seq analysis of FACS-sorted Day 9 P1, Day 9 P2, Day 15 P1, and Day 15 P2 stromal cells from WT mouse colons (n = 4 per group) during early life. **(a)** Principal component analysis (PCA) of the four groups of stromal cell populations from the colon lamina propria. **(b, c)** Top eight Gene Ontology (GO) pathway annotations for the 1,052 significantly differentially expressed genes (DEGs) ($P_{adj} < 0.05$, $\log_2|FC| > 1$, avgTPM > 10) uniquely dysregulated in P1 stromal cells between Day 9 and Day 15. GO terms for genes upregulated in Day 15 P1 **(b)** and Day 9 P1 **(c)** stromal cells. **(d)** Normalized *Bmp2* expression levels across Day 9 P1, Day 15 P1, Day 9 P2, and Day 15 P2 stromal cells (n = 4 per group). **(e)** Feature plot of *Bmp2* expression in Day 9 scRNA-seq data. Red circles indicate P1 (*Wnt4*$^+$) stromal cells; blue circles indicate P2 (other) stromal cells. **(f, g)** Bulk RNA-seq analysis of FACS-sorted Day 9 iNKT cells and conventional TCR-αβ T (αβT) cells from WT mouse colons (n = 4 per group). **(f)** Top eight GO pathway annotations for genes upregulated in Day 9 iNKT cells compared to αβT cells. **(g)** Heatmap of representative gene expression levels associated with MAPK signaling and integrin-mediated cell adhesion. Data are presented as $\log_2$(TPM +1) for visualization. Each column represents an individual RNA-seq library. **(h)** Flow cytometry analysis of BMPR1A, BMPR1B, and BMPR2 surface expression on αβT and iNKT cells from Day 9 and Day 15 WT mouse colons (n = 6). **(i, j)** Absolute iNKT cell numbers and Ki67 mean fluorescence intensity (MFI) of thymic CD1d tetramer-positive iNKT cells under different conditions: **(i)** Cultured with 0, 50, or 100 ng/ml mouse recombinant BMP2 (mrBMP2) for 3 days (n = 4 per group), **(j)** Co-cultured with P1 stromal cells and treated with either a vehicle control (Veh) or BMP signaling inhibitor Dorsomorphin (Dor) for 3 days (n = 6 per group). **(k, l)** Absolute αβT cell and iNKT cell numbers and iNKT Ki67 MFI in mouse colons following in vivo intraperitoneal (IP) injection of vehicle control (Veh) or Dorsomorphin (Dor) during **(k)** Early-life (Day 6-12, Dor6-12 H13), created in BioRender. Hanley, T. (2026) https://BioRender.com/kjhpgc7 or **(l)** Later-life (Day 16-22, Dor16-22 H23), created in BioRender. Hanley, T. (2026) https://BioRender.com/u8kys5c. Data are presented as mean ± SD. *P* values were calculated by one-way ANOVA with Dunnett's multiple comparisons test **(d, i)**, two-way ANOVA with Tukey's multiple comparisons test **(h)**, and unpaired two-sided Student's t-test **(j-l)**. $P < 0.05$ is considered statistically significant. Each symbol **(h-l)** represents one individual mouse. Data **(h-l)** are representative of three independent experiments. Source data are provided as a Source Data file.

Fig. 4 | Identification of an embryonic macrophage-P1 (*Wnt4*$^+$) stromal cell-iNKT cell niche in the early-life mouse colon. (a) TPM (Transcripts Per Million) expression of *Foxl1* in bulk RNA-seq of Day 9 P1 and P2 stromal cells (each group, n=4). **(b)** Feature plot of *Foxl1* expression in Day 9 scRNA-seq data. Red circles indicate P1 (*Wnt4*$^+$) stromal cells, and the blue circle indicates P2 (other) stromal cells. **(c-d)** Flow cytometry analysis of Day 9 *Foxl1-CreER*^{T2}*-tdTomato* mice (n=5). **(c)** Proportion of CD34$^-$CD9$^-$ P1 stromal cells (~80%) and CD34$^+$CD9$^+$ P2 stromal cells (~10%) among all tdTomato$^+$ stromal cells. **(d)** Percentage of tdTomato$^+$ cells in CD34$^-$CD9$^-$ P1 and CD34$^+$CD9$^+$ P2 stromal cell populations in *Foxl1-CreER*^{T2}*-tdTomato* mice (n=5, orange) and littermate controls (n=5, black). **(e)** Representative confocal images of Day 9 *Foxl1-CreER*^{T2}*-tdTomato* mice mouse colon stained with anti-tdTomato (red, P1 stromal cells), anti-PDGFRA (green, all stromal cells), and DAPI (blue). Scale bar, 200 μm. **(f)** Schematic of the CD45.1$^+$ thymic iNKT cell isolation and adoptive transfer strategy. Created in BioRender. Hanley, T. (2026) https://BioRender.com/u5yd48q. **(g)** Representative confocal images of Day 10 CD45.2 WT colon stained with anti-CD45.1 (red, iNKT cells) and DAPI (blue), with or without CD45.1 iNKT cell adoptive transfer. Scale bar, 100 μm. **(h)** Representative confocal images of Day 10 CD45.2 *Foxl1-CreER*^{T2}*-tdTomato*; *Cx3cr1-GFP* mouse colon stained with anti-tdTomato (red, P1 stromal cells), anti-GFP (green, macrophages), and anti-CD45.1 (blue, iNKT cells), with or without CD45.1 iNKT cell adoptive transfer. Scale bar, 50 μm. White arrows indicate transferred CD45.1$^+$ iNKT cells, and dashed gray lines denote the interface between the mucosa and muscular layers. **(i)** Quantification of total CD45.1$^+$ iNKT cells located in the LP crypt region within the niche together with macrophage and P1 stromal cells, or located in the submucosa and muscularis layers, separate from macrophage and P1 stromal cells, in each transferred mouse (n=4). Data are presented as mean ± SD; *P* values were calculated by unpaired two-sided Student's t-test **(a, c, i)**, two-way ANOVA corrected with Tukey's multiple comparisons test **(d)**. $P < 0.05$ is considered statistically significant. Each symbol **(c, d, i)** represents one individual mouse. Data **(c, d, i)** are representative of three independent experiments. Source data are provided as a Source Data file.

Fig. 5 | Early-life P1 (*Wnt4*$^+$) stromal cell-specific depletion of BMP2 inhibits colonic iNKT cell accumulation, influencing disease susceptibility in adulthood. Schematic of the P1 stromal cell-specific BMP2 depletion models, **(a)** depletion from Day 6-12, tissue harvest at Day 13, created in BioRender. Hanley, T. (2026) https://BioRender.com/rjjyckx, **(d)** depletion from Day 6-8, tissue harvest at Day 9, created in BioRender. Hanley, T. (2026) https://BioRender.com/m7yrzff, **(f)** depletion from Day 14-20, tissue harvest at Day 21, created in BioRender. Hanley, T. (2026) https://BioRender.com/sut2jb1, **(h)** depletion from Day 6-12, tissue harvest at Day 56, created in BioRender. Hanley, T. (2026) https://BioRender.com/sygoydi. **(b, c)** Representative flow cytometry plots and quantification of absolute cell numbers and Ki67 mean fluorescence intensity (MFI) of colonic iNKT cells **(b),** absolute cell numbers of colonic P1 and P2 stromal cells,

macrophages, and conventional αβ T cells **(c)** in Day 13 littermate control (Foxl1^{CreER-}, n=5) and Day 6-12 P1 BMP2-depleted (Foxl1^{CreER+}, n=5) mice. **(e)** Representative flow cytometry plots (left) and quantification of absolute cell numbers and Ki67 MFI of colonic iNKT cells in Day 9 littermate control (Foxl1^{CreER-}, n=5) and Day 6-8 P1 BMP2-depleted (Foxl1^{CreER+}, n=5) mice. **(g)** Representative flow cytometry plots (left) and quantification of absolute cell numbers and Ki67 MFI of colonic iNKT cells in Day 21 littermate control (Foxl1^{CreER-}, n=6) and Day 14-20 P1 BMP2-depleted (Foxl1^{CreER+}, n=6) mice. **(i)** Representative flow cytometry plots (left) and quantification of absolute cell numbers and Ki67 MFI of colonic iNKT cells in Day 56 littermate control (Foxl1^{CreER-}, n=9) and Day 6-12 P1 BMP2-depleted (Foxl1^{CreER+}, n=7) mice. **(j, m)** Schematic representation of the experimental models following Day 6-12 P1 BMP2 depletion: **(j)** oxazolone-induced colitis, created in BioRender. Hanley, T. (2026) https://BioRender.com/kaqw3vz, and **(m)** *Listeria monocytogenes* infection, created in BioRender. Hanley, T. (2026) https://BioRender.com/lfmkidd. **(k, l)** Intrarectal administration of oxazolone (Oxa, 1% Oxa/50% EtOH) or ethanol control (EtOH, 50% EtOH) on Day 56, with assessment of colitis severity in littermate controls (Foxl1^{CreER-}) and Day 6-12 P1 BMP2-depleted (Foxl1^{CreER+}) mice 3 days post-treatment (Day 59). **(k)** Body weight loss; **(l)** representative H&E-stained colon sections and quantitative pathology scoring (Foxl1^{CreER-}: EtOH n=11, Oxa n=11; Foxl1^{CreER+}: EtOH n=14, Oxa n=15). Scale bar, 200 μm. **(n)** Oral gavage of *L. monocytogenes* on Day 56, with bacterial colony-forming unit (CFU) quantification in the colon, ileum, and mesenteric lymph nodes (mLN) of littermate controls (Foxl1^{CreER-}, n=16) and Day 6-12 P1 BMP2-depleted (Foxl1^{CreER+}, n=11) mice on Day 59. Blue and red dots indicate *Foxl1^{CreER-}Bmp2$^{fl/fl}$* and *Foxl1^{CreER+}Bmp2$^{fl/fl}$* mice, respectively. Data are presented as mean ± SD; *P* values were calculated by unpaired two-sided Student's *t*-test **(b, c, e, g, i)**, two-way ANOVA with Tukey's **(k)** and Sidak's **(n)** multiple comparisons test, and one-way ANOVA with Dunnett's multiple comparisons test **(l)**. $P < 0.05$ is considered statistically significant. Each symbol represents one individual mouse. Data are representative of three independent experiments **(b-i)** or pooled from three independent experiments **(k, l, n)**. Source data are provided as a Source Data file.

Fig. 6 | Germ-reduced mice exhibit increased P1 (*Wnt4*$^{+}$) stromal cell number and BMP2 production during early-life, associated with excessive colonic iNKT cell accumulation. (a) Representative flow cytometry plots (left) and quantification of absolute cell numbers of Day 9 and Day 15 P1 stromal cells in specific pathogen-free (SPF, n=5) and germ-free (GF, n=6) wild-type (WT) mice. **(b)** Quantitative PCR analysis of *Wnt4* and *Bmp2* expression in FACS-sorted Day 9 P1 and P2 stromal cells from SPF (n=6) and GF (n=6) WT mice. **(c)** Schematic of early-life antibiotic treatment (Abx) in *Foxl1^{CreER}Bmp2$^{fl/fl}$* mice from birth (Day 0) to Day 21, combined with P1 stromal cell-specific *Bmp2* deletion via tamoxifen (TAM) administration from Day 6 to Day 12. Colon tissues were collected on Days 9, 13, and 56 for iNKT cell analysis. Created in BioRender. Hanley, T. (2026) https://BioRender.com/pi0p68q. Symbols shown for panels **d-f**. **(d-f)**

Representative flow cytometry plots (left) and quantification of **(d)** Ki67 mean fluorescence intensity (MFI) in Day 9 colonic iNKT cells (SPF Foxl1^{CreER-}, n=6; SPF Foxl1^{CreER+}, n=8; Abx Foxl1^{CreER-}, n=7; Abx Foxl1^{CreER+}, n=9), **(e)** absolute cell numbers of Day 13 colonic iNKT cells (SPF Foxl1^{CreER-}, n=6; SPF Foxl1^{CreER+}, n=5; Abx Foxl1^{CreER-}, n=8; Abx Foxl1^{CreER+}, n=10), and **(f)** absolute cell numbers of Day 56 colonic iNKT cells (SPF Foxl1^{CreER-}, n=10; SPF Foxl1^{CreER+}, n=9; Abx Foxl1^{CreER-}, n=9; Abx Foxl1^{CreER+}, n=12) in untreated (SPF) and early-life antibiotic-treated (Abx) littermate control (*Foxl1^{CreER-}Bmp2$^{fl/fl}$*) and P1 BMP2-depleted (*Foxl1^{CreER+}Bmp2$^{fl/fl}$*) mice. **(g-i)** Intrarectal injection of oxazolone (Oxa) or ethanol control (EtOH) at Day 56, followed by colitis severity assessment in SPF or Abx-treated *Foxl1^{CreER-}Bmp2$^{fl/fl}$* and *Foxl1^{CreER+}Bmp2$^{fl/fl}$* mice (SPF Foxl1^{CreER-}: EtOH, n=7; Oxa, n=8; SPF Foxl1^{CreER+}: EtOH, n=8; Oxa, n=11; Abx Foxl1^{CreER-}: EtOH, n=8; Oxa, n=8; Abx Foxl1^{CreER+}: EtOH, n=6; Oxa, n=8) three days post-injection (Day 59) via **(g)** body weight loss, **(h)** quantitative pathology scoring, and **(i)** representative colon H&E staining. Scale bar, 200 μm. Grey dots and orange squares indicate *Foxl1^{CreER-}Bmp2$^{fl/fl}$* and *Foxl1^{CreER+}Bmp2$^{fl/fl}$* mice, respectively. Data are presented as mean ± SD. *P* values were calculated by two-way ANOVA with Tukey's multiple comparisons test **(a, b, g)**, and one-way ANOVA with Dunnett's multiple comparisons test **(d-f, h)**. $P < 0.05$ is considered statistically significant. Each symbol represents one individual mouse. Data are representative of three independent experiments **(a, b)** or pooled from three independent experiments **(d-h)**. Source data are provided as a Source Data file.

Fig. 7 | Identification of an ortholog of P1 stromal cell population in early-life human colon and BMP2-mediated promotion of human iNKT cell proliferation. (a-d) Single-cell RNA-seq analysis of fibroblastic cells from the fetal human colon (21 samples, 8-22 post-conceptual weeks, total 15,540 cells). **(a)** Unsupervised UMAP clustering. **(b)** Dot plot displaying the expression of key marker genes associated with Day 9 mouse colon P1 (*Wnt4*$^+$) stromal cells in fetal human stromal clusters. The red arrow indicates enrichment in cluster 1. **(c)** Heatmap showing the expression of genes specifically enriched in mouse P1 stromal cells (C1 *Wnt4*$^+$ and C8 *Fgf9*$^+$ stromal cells), which are predominantly expressed in human cluster 1 (red arrow). **(d)** Expression of a gene module comprising human orthologs of the top 20 feature genes identified in *Wnt4*$^+$ stromal cells of the Day 9 mouse colon. Cluster 1 (red arrow) exhibits significantly higher expression ($P_{adj} < 0.0001$) compared to the other four stromal clusters. Adjusted P values were calculated using a two-sided Wilcoxon rank-sum test with Benjamini–Hochberg correction. **(e)** Spatial expression patterns of *EPCAM, PDGFRA, ADAMDEC1, CXCL14*, and *BMP2* in the neonatal (2-month-old) human colon, as detected by MERSCOPE. Scale bar, 500 μm. **(f)** Surface expression of BMPR1B on the human CD4$^+$ iNKT cell WINK3b.1. Grey and red histograms and dots represent the isotype control and anti-hBMPR1B staining, respectively. **(g)** Cell survival, proliferation (Ki67 MFI), and cell number of WINK3b.1 iNKT cells following treatment with recombinant human BMP2 (0, 50, 100 ng/ml) for 2 days.

Data are presented as mean ± SD; *P* values were calculated by unpaired two-sided Student's *t*-test **(f)** and one-way ANOVA with Dunnett's multiple comparisons test **(g)**. $P < 0.05$ is considered statistically significant. Data **(f, g)** are representative of three independent experiments. Source data are provided as a Source Data file.

Editor's Summary

How early-life intestinal microenvironment shape colonic iNKT cell development to be further explored. The authors here identify an early-life enriched $Wnt4^{+}$ stromal cells form a microbiota-regulated neonatal niche that drives iNKT expansion via BMP2-MAPK signaling and programs long term mucosal immune homeostasis.

Peer review information: *Nature Communications* thanks the anonymous reviewer(s) for their contribution to the peer review of this work. A peer review file is available.

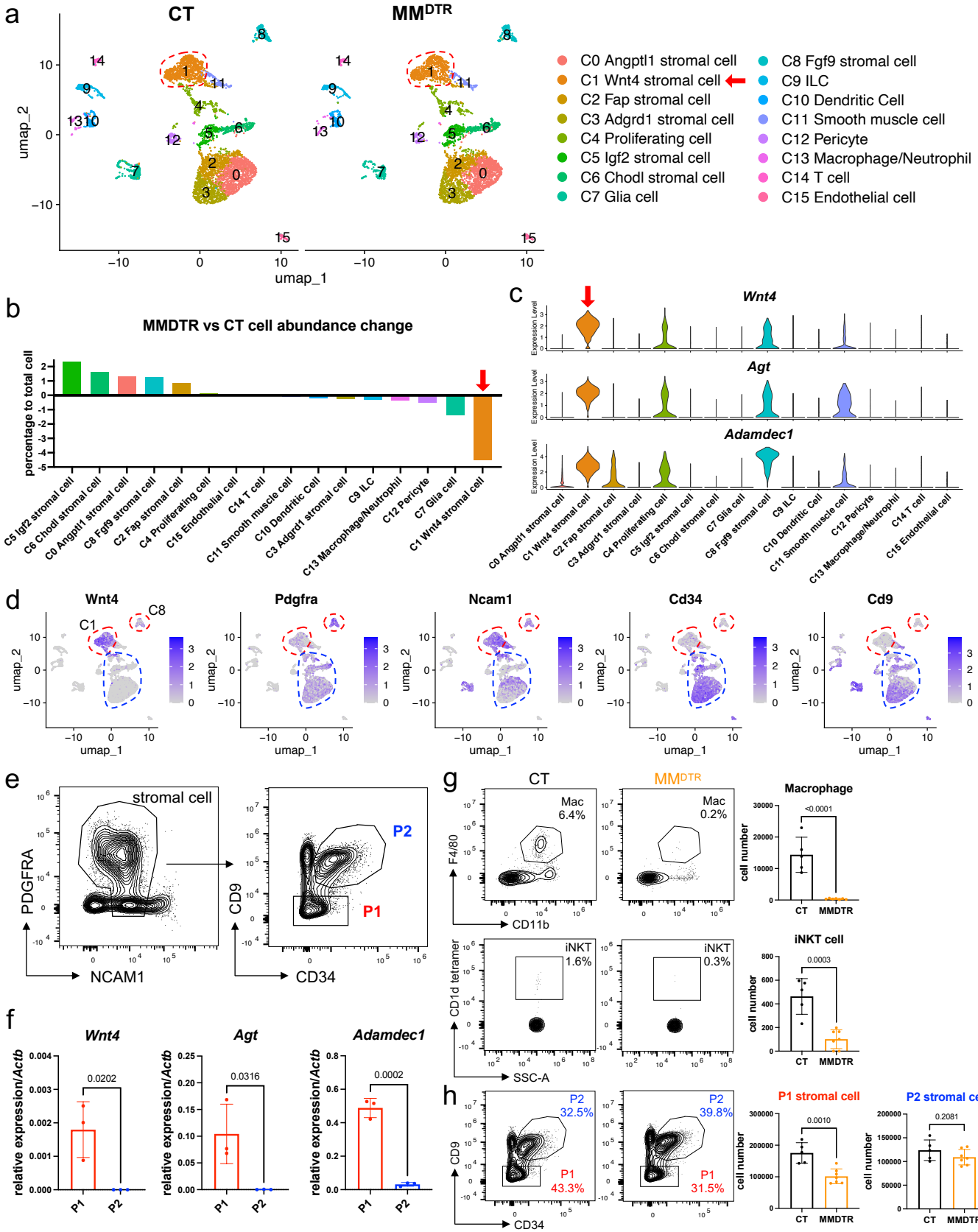
a
CT
MMDTR
umap_2
umap_1
C0 Angptl1 stromal cell
C1 Wnt4 stromal cell
C2 Fap stromal cell
C3 Adgrd1 stromal cell
C4 Proliferating cell
C5 Igf2 stromal cell
C6 Chodl stromal cell
C7 Glia cell
C8 Fgf9 stromal cell
C9 ILC
C10 Dendritic Cell
C11 Smooth muscle cell
C12 Pericyte
C13 Macrophage/Neutrophil
C14 T cell
C15 Endothelial cell
b
MMDTR vs CT cell abundance change
percentage to total cell
c
Wnt4
Agt
Adamdec1
Expression Level
d
Wnt4
Pdgfra
Ncam1
Cd34
Cd9
C1
C8
e
stromal cell
PDGFRA
NCAM1
CD9
CD34
P1
P2
f
Wnt4
Agt
Adamdec1
relative expression/Actb
0.0202
0.0316
0.0002
g
CT
MMDTR
F4/80
CD11b
Mac
6.4%
0.2%
Macrophage
cell number
<0.0001
CD1d tetramer
SSC-A
iNKT
1.6%
0.3%
iNKT cell
0.0003
h
CD9
CD34
P2
32.5%
39.8%
P1
43.3%
31.5%
P1 stromal cell
0.0010
P2 stromal cell
0.2081

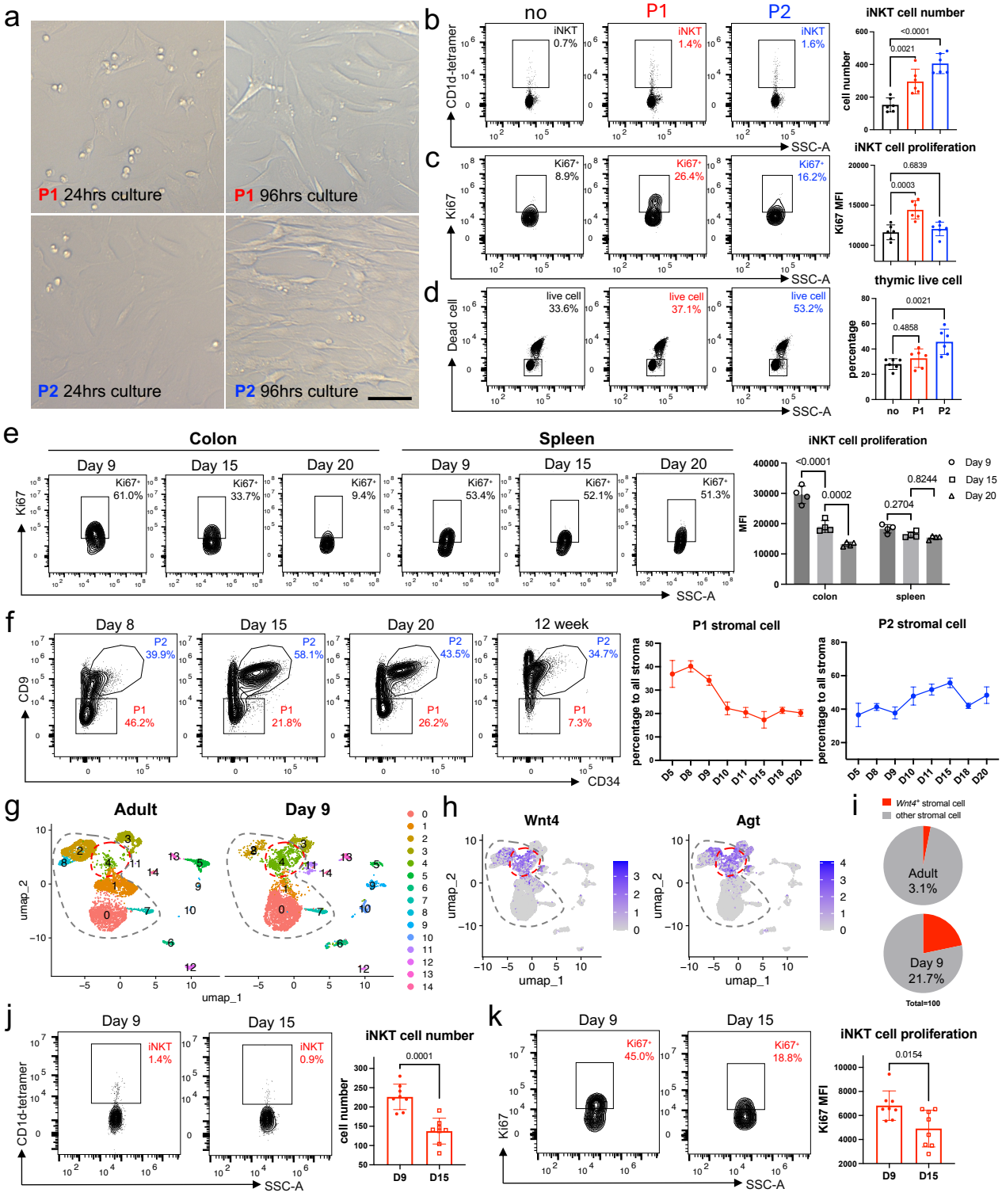
a
P1 24hrs culture
P1 96hrs culture
P2 24hrs culture
P2 96hrs culture
b
no
P1
P2
CD1d-tetramer
iNKT 0.7%
iNKT 1.4%
iNKT 1.6%
SSC-A
iNKT cell number
cell number
<0.0001
0.0021
c
Ki67
Ki67+ 8.9%
Ki67+ 26.4%
Ki67+ 16.2%
iNKT cell proliferation
Ki67 MFI
0.6839
0.0003
d
Dead cell
live cell 33.6%
live cell 37.1%
live cell 53.2%
thymic live cell
percentage
0.0021
0.4858
e
Colon
Spleen
Day 9
Day 15
Day 20
Ki67+ 61.0%
Ki67+ 33.7%
Ki67+ 9.4%
Ki67+ 53.4%
Ki67+ 52.1%
Ki67+ 51.3%
iNKT cell proliferation
MFI
<0.0001
0.0002
0.8244
0.2704
colon
spleen
f
Day 8
Day 15
Day 20
12 week
CD9
CD34
P2 39.9%
P1 46.2%
P2 58.1%
P1 21.8%
P2 43.5%
P1 26.2%
P2 34.7%
P1 7.3%
P1 stromal cell
P2 stromal cell
percentage to all stroma
g
Adult
Day 9
umap_1
umap_2
h
Wnt4
Agt
i
Wnt4+ stromal cell
other stromal cell
Adult 3.1%
Day 9 21.7%
Total=100
j
Day 9
Day 15
iNKT 1.4%
iNKT 0.9%
iNKT cell number
0.0001
D9
D15
k
Day 9
Day 15
Ki67+ 45.0%
Ki67+ 18.8%
iNKT cell proliferation
0.0154

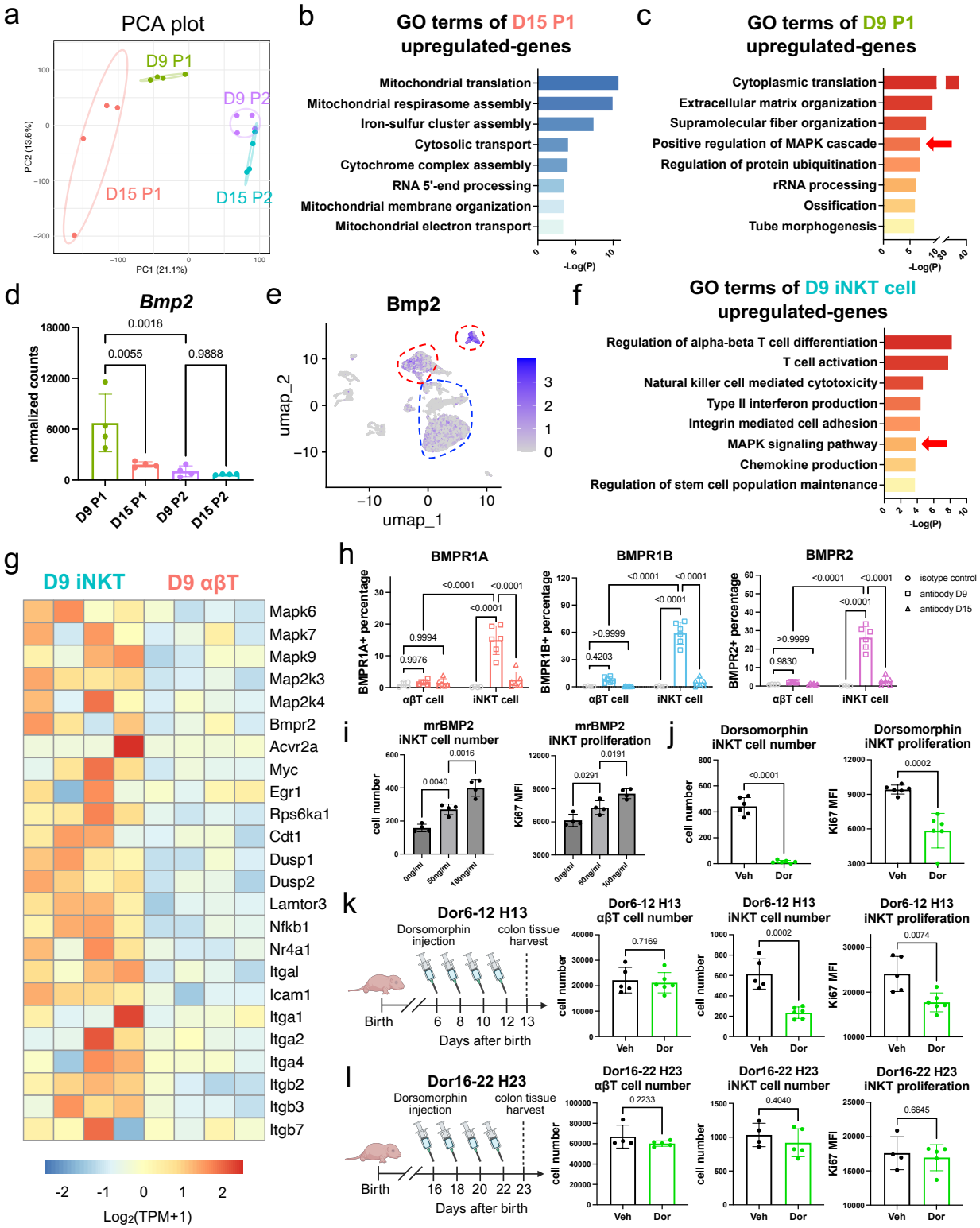
a
PCA plot
D9 P1
D9 P2
D15 P1
D15 P2
PC1 (21.1%)
PC2 (13.6%)
b
GO terms of D15 P1 upregulated-genes
Mitochondrial translation
Mitochondrial respirasome assembly
Iron-sulfur cluster assembly
Cytosolic transport
Cytochrome complex assembly
RNA 5'-end processing
Mitochondrial membrane organization
Mitochondrial electron transport
-Log(P)
c
GO terms of D9 P1 upregulated-genes
Cytoplasmic translation
Extracellular matrix organization
Supramolecular fiber organization
Positive regulation of MAPK cascade
Regulation of protein ubiquitination
rRNA processing
Ossification
Tube morphogenesis
-Log(P)
d
Bmp2
normalized counts
0.0018
0.0055
0.9888
D9 P1
D15 P1
D9 P2
D15 P2
e
Bmp2
umap_1
umap_2
f
GO terms of D9 iNKT cell upregulated-genes
Regulation of alpha-beta T cell differentiation
T cell activation
Natural killer cell mediated cytotoxicity
Type II interferon production
Integrin mediated cell adhesion
MAPK signaling pathway
Chemokine production
Regulation of stem cell population maintenance
-Log(P)
g
D9 iNKT
D9 αβT
Mapk6
Mapk7
Mapk9
Map2k3
Map2k4
Bmpr2
Acvr2a
Myc
Egr1
Rps6ka1
Cdt1
Dusp1
Dusp2
Lamtor3
Nfkb1
Nr4a1
Itgal
Icam1
Itga1
Itga2
Itga4
Itgb2
Itgb3
Itgb7
Log2(TPM+1)
h
BMPR1A
BMPR1B
BMPR2
BMPR1A+ percentage
BMPR1B+ percentage
BMPR2+ percentage
αβT cell
iNKT cell
isotype control
antibody D9
antibody D15
i
mrBMP2 iNKT cell number
mrBMP2 iNKT proliferation
cell number
Ki67 MFI
0ng/ml
50ng/ml
100ng/ml
j
Dorsomorphin iNKT cell number
Dorsomorphin iNKT proliferation
Veh
Dor
k
Dor6-12 H13
Dorsomorphin injection
colon tissue harvest
Birth
Days after birth
Dor6-12 H13 αβT cell number
Dor6-12 H13 iNKT cell number
Dor6-12 H13 iNKT proliferation
l
Dor16-22 H23
Dorsomorphin injection
colon tissue harvest
Birth
Days after birth
Dor16-22 H23 αβT cell number
Dor16-22 H23 iNKT cell number
Dor16-22 H23 iNKT proliferation

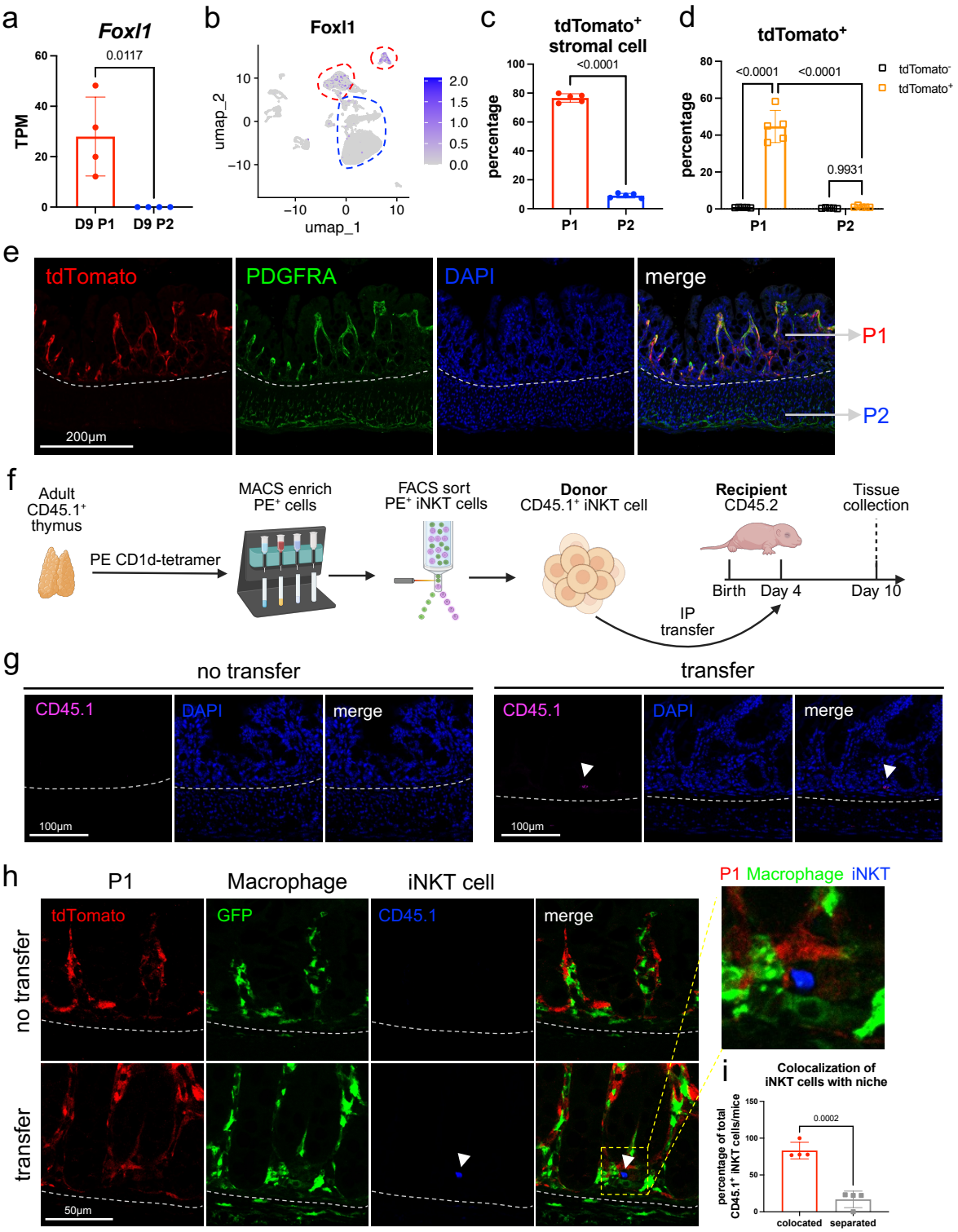
a
Foxl1
0.0117
TPM
D9 P1
D9 P2
b
Foxl1
umap_2
umap_1
c
tdTomato+ stromal cell
<0.0001
percentage
P1
P2
d
tdTomato+
<0.0001
<0.0001
0.9931
tdTomato-
tdTomato+
e
tdTomato
PDGFRA
DAPI
merge
200µm
P1
P2
f
Adult CD45.1+ thymus
PE CD1d-tetramer
MACS enrich PE+ cells
FACS sort PE+ iNKT cells
Donor CD45.1+ iNKT cell
Recipient CD45.2
Tissue collection
Birth
Day 4
Day 10
IP transfer
g
no transfer
transfer
CD45.1
DAPI
merge
100µm
h
P1
Macrophage
iNKT cell
no transfer
transfer
tdTomato
GFP
CD45.1
merge
50µm
P1 Macrophage iNKT
i
Colocalization of iNKT cells with niche
percentage of total CD45.1+ iNKT cells/mice
0.0002
colocated
separated

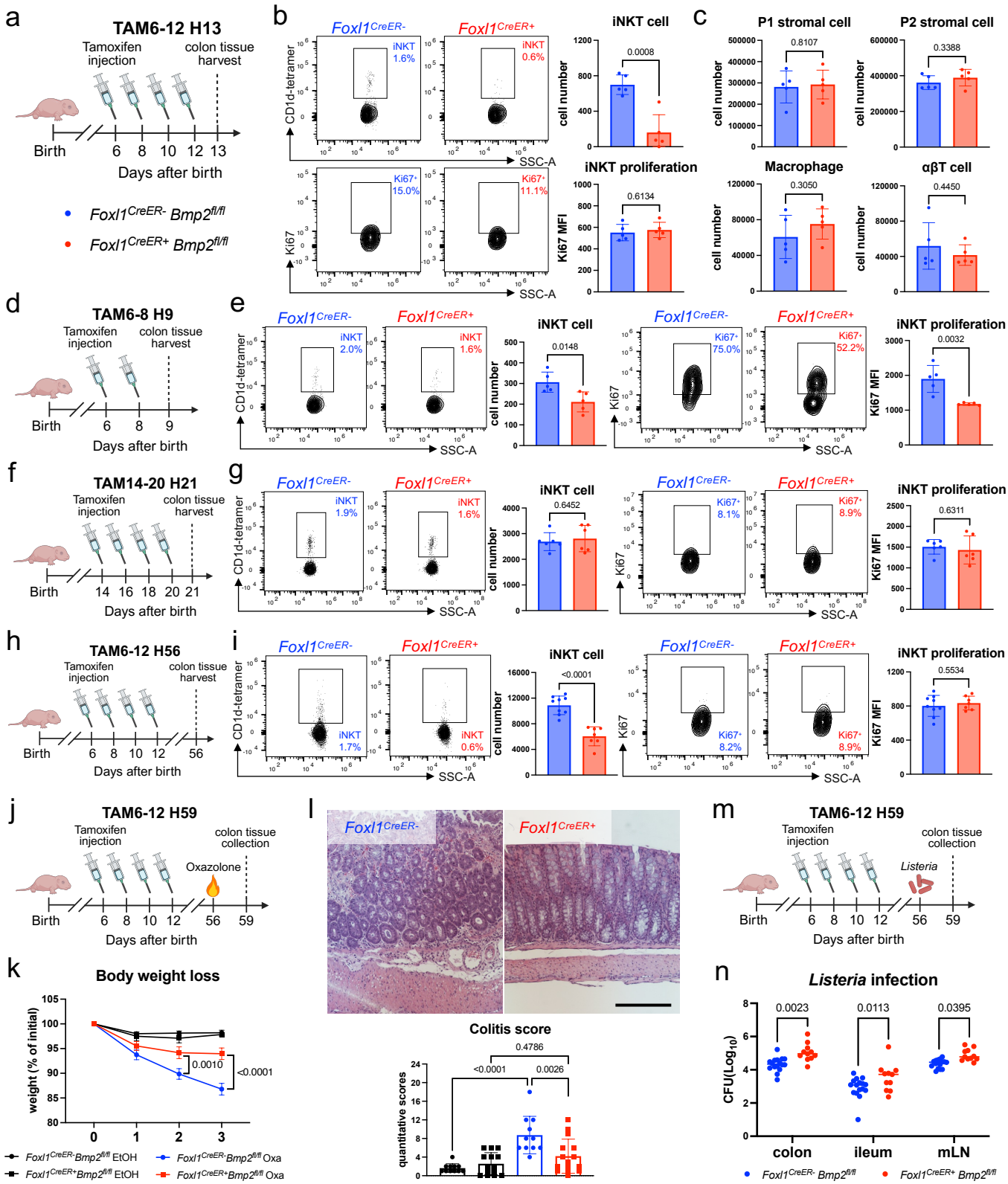
a
TAM6-12 H13
Tamoxifen injection
colon tissue harvest
Birth
6 8 10 12 13
Days after birth
Foxl1CreER- Bmp2fl/fl
Foxl1CreER+ Bmp2fl/fl
b
Foxl1CreER-
Foxl1CreER+
iNKT 1.6%
iNKT 0.6%
CD1d-tetramer
SSC-A
Ki67+ 15.0%
Ki67+ 11.1%
Ki67
iNKT cell
0.0008
cell number
iNKT proliferation
0.6134
Ki67 MFI
c
P1 stromal cell
0.8107
P2 stromal cell
0.3388
Macrophage
0.3050
αβT cell
0.4450
d
TAM6-8 H9
Tamoxifen injection
colon tissue harvest
Birth
6 8 9
Days after birth
e
iNKT 2.0%
iNKT 1.6%
0.0148
Ki67+ 75.0%
Ki67+ 52.2%
0.0032
f
TAM14-20 H21
Tamoxifen injection
colon tissue harvest
Birth
14 16 18 20 21
Days after birth
g
iNKT 1.9%
iNKT 1.6%
0.6452
Ki67+ 8.1%
Ki67+ 8.9%
0.6311
h
TAM6-12 H56
Tamoxifen injection
colon tissue harvest
Birth
6 8 10 12 56
Days after birth
i
iNKT 1.7%
iNKT 0.6%
<0.0001
Ki67+ 8.2%
Ki67+ 8.9%
0.5534
j
TAM6-12 H59
Tamoxifen injection
colon tissue collection
Oxazolone
Birth
6 8 10 12 56 59
Days after birth
k
Body weight loss
weight (% of initial)
0.0010
<0.0001
Foxl1CreER-Bmp2fl/fl EtOH
Foxl1CreER+Bmp2fl/fl EtOH
Foxl1CreER-Bmp2fl/fl Oxa
Foxl1CreER+Bmp2fl/fl Oxa
l
Foxl1CreER-
Foxl1CreER+
Colitis score
quantitative scores
0.4786
<0.0001
0.0026
m
TAM6-12 H59
Tamoxifen injection
colon tissue collection
Listeria
Birth
6 8 10 12 56 59
Days after birth
n
Listeria infection
CFU(Log10)
0.0023
0.0113
0.0395
colon
ileum
mLN
Foxl1CreER- Bmp2fl/fl
Foxl1CreER+ Bmp2fl/fl

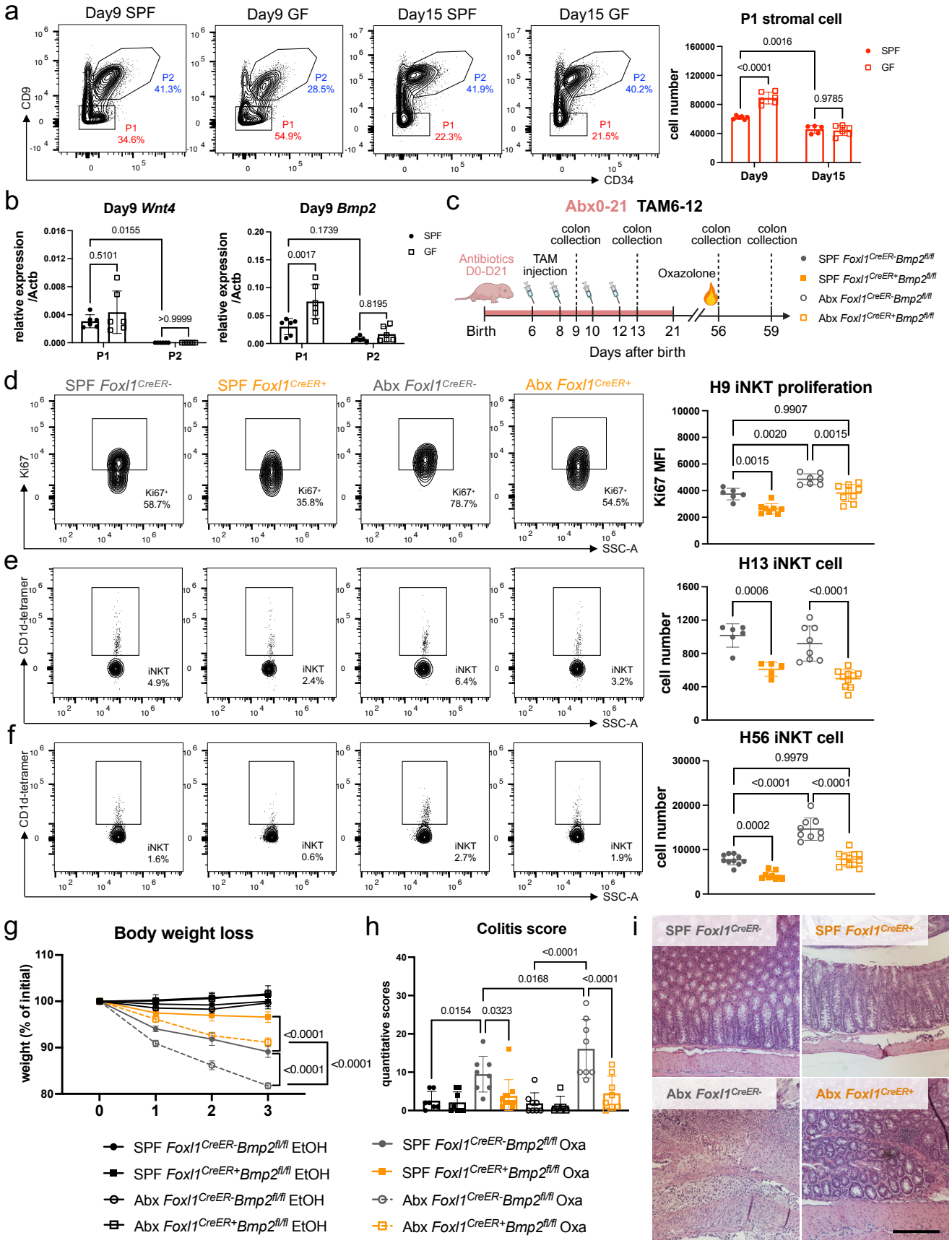
a
Day9 SPF
Day9 GF
Day15 SPF
Day15 GF
CD9
CD34
P1
34.6%
P2
41.3%
54.9%
28.5%
22.3%
41.9%
21.5%
40.2%
P1 stromal cell
cell number
0.0016
<0.0001
0.9785
SPF
GF
Day9
Day15
b
Day9 Wnt4
Day9 Bmp2
relative expression /Actb
0.0155
0.5101
>0.9999
0.1739
0.0017
0.8195
P1
P2
SPF
GF
c
Abx0-21
TAM6-12
Antibiotics D0-D21
TAM injection
colon collection
Oxazolone
Birth
Days after birth
SPF Foxl1CreER-Bmp2fl/fl
SPF Foxl1CreER+Bmp2fl/fl
Abx Foxl1CreER-Bmp2fl/fl
Abx Foxl1CreER+Bmp2fl/fl
d
SPF Foxl1CreER-
SPF Foxl1CreER+
Abx Foxl1CreER-
Abx Foxl1CreER+
Ki67
SSC-A
Ki67+ 58.7%
Ki67+ 35.8%
Ki67+ 78.7%
Ki67+ 54.5%
H9 iNKT proliferation
Ki67 MFI
0.9907
0.0020
0.0015
e
CD1d-tetramer
iNKT 4.9%
iNKT 2.4%
iNKT 6.4%
iNKT 3.2%
H13 iNKT cell
0.0006
<0.0001
f
iNKT 1.6%
iNKT 0.6%
iNKT 2.7%
iNKT 1.9%
H56 iNKT cell
0.9979
<0.0001
0.0002
g
Body weight loss
weight (% of initial)
<0.0001
h
Colitis score
quantitative scores
0.0154
0.0323
0.0168
SPF Foxl1CreER-Bmp2fl/fl EtOH
SPF Foxl1CreER+Bmp2fl/fl EtOH
Abx Foxl1CreER-Bmp2fl/fl EtOH
Abx Foxl1CreER+Bmp2fl/fl EtOH
SPF Foxl1CreER-Bmp2fl/fl Oxa
SPF Foxl1CreER+Bmp2fl/fl Oxa
Abx Foxl1CreER-Bmp2fl/fl Oxa
Abx Foxl1CreER+Bmp2fl/fl Oxa
i
SPF Foxl1CreER-
SPF Foxl1CreER+
Abx Foxl1CreER-
Abx Foxl1CreER+

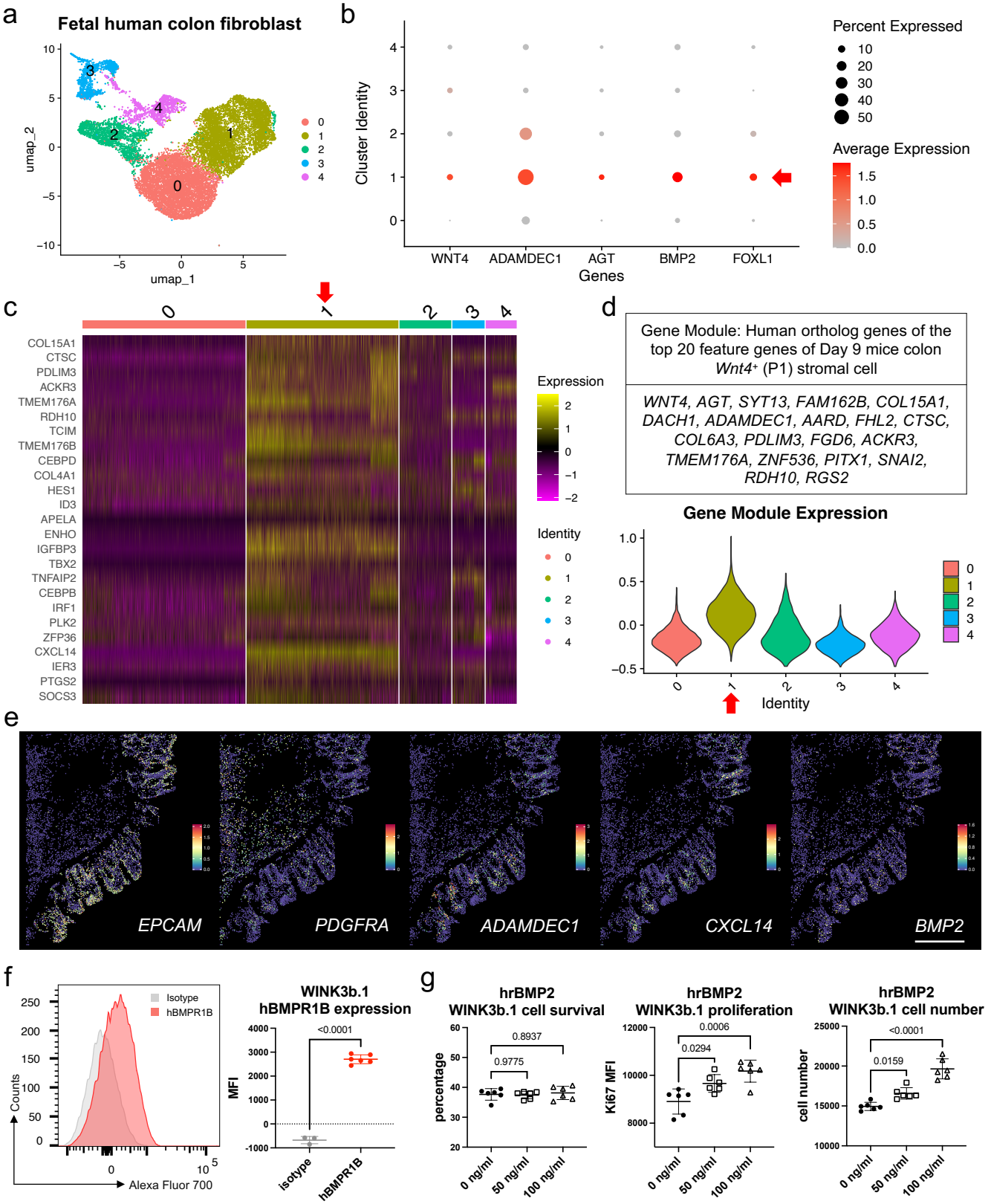
a
Fetal human colon fibroblast
umap_2
umap_1
0
1
2
3
4
b
Cluster Identity
WNT4
ADAMDEC1
AGT
BMP2
FOXL1
Genes
Percent Expressed
Average Expression
c
COL15A1
CTSC
PDLIM3
ACKR3
TMEM176A
RDH10
TCIM
TMEM176B
CEBPD
COL4A1
HES1
ID3
APELA
ENHO
IGFBP3
TBX2
TNFAIP2
CEBPB
IRF1
PLK2
ZFP36
CXCL14
IER3
PTGS2
SOCS3
Expression
Identity
d
Gene Module: Human ortholog genes of the top 20 feature genes of Day 9 mice colon Wnt4+ (P1) stromal cell
WNT4, AGT, SYT13, FAM162B, COL15A1, DACH1, ADAMDEC1, AARD, FHL2, CTSC, COL6A3, PDLIM3, FGD6, ACKR3, TMEM176A, ZNF536, PITX1, SNAI2, RDH10, RGS2
Gene Module Expression
Identity
e
EPCAM
PDGFRA
ADAMDEC1
CXCL14
BMP2
f
Isotype
hBMPR1B
Counts
Alexa Fluor 700
WINK3b.1
hBMPR1B expression
MFI
<0.0001
isotype
hBMPR1B
g
hrBMP2
WINK3b.1 cell survival
percentage
0.8937
0.9775
hrBMP2
WINK3b.1 proliferation
Ki67 MFI
0.0006
0.0294
hrBMP2
WINK3b.1 cell number
cell number
<0.0001
0.0159
0 ng/ml
50 ng/ml
100 ng/ml